INFORMATION TO USERS

This manuscript has been reproduced from the microfilm master. UMI films the text directly from the original or copy submitted. Thus, some thesis and dissertation copies are in typewriter face, while others may be from any type of computer printer.

The quality of this reproduction is dependent upon the quality of the copy submitted. Broken or indistinct print, colored or poor quality illustrations and photographs, print bleedthrough, substandard margins, and improper alignment can adversely affect reproduction.

In the unlikely event that the author did not send UMI a complete manuscript and there are missing pages, these will be noted. Also, if unauthorized copyright material had to be removed, a note will indicate the deletion.

Oversize materials (e.g., maps, drawings, charts) are reproduced by sectioning the original, beginning at the upper left-hand corner and continuing from left to right in equal sections with small overlaps.

ProQuest Information and Learning
300 North Zeeb Road, Ann Arbor, MI 48106-1346 USA
800-521-0600

UMI®

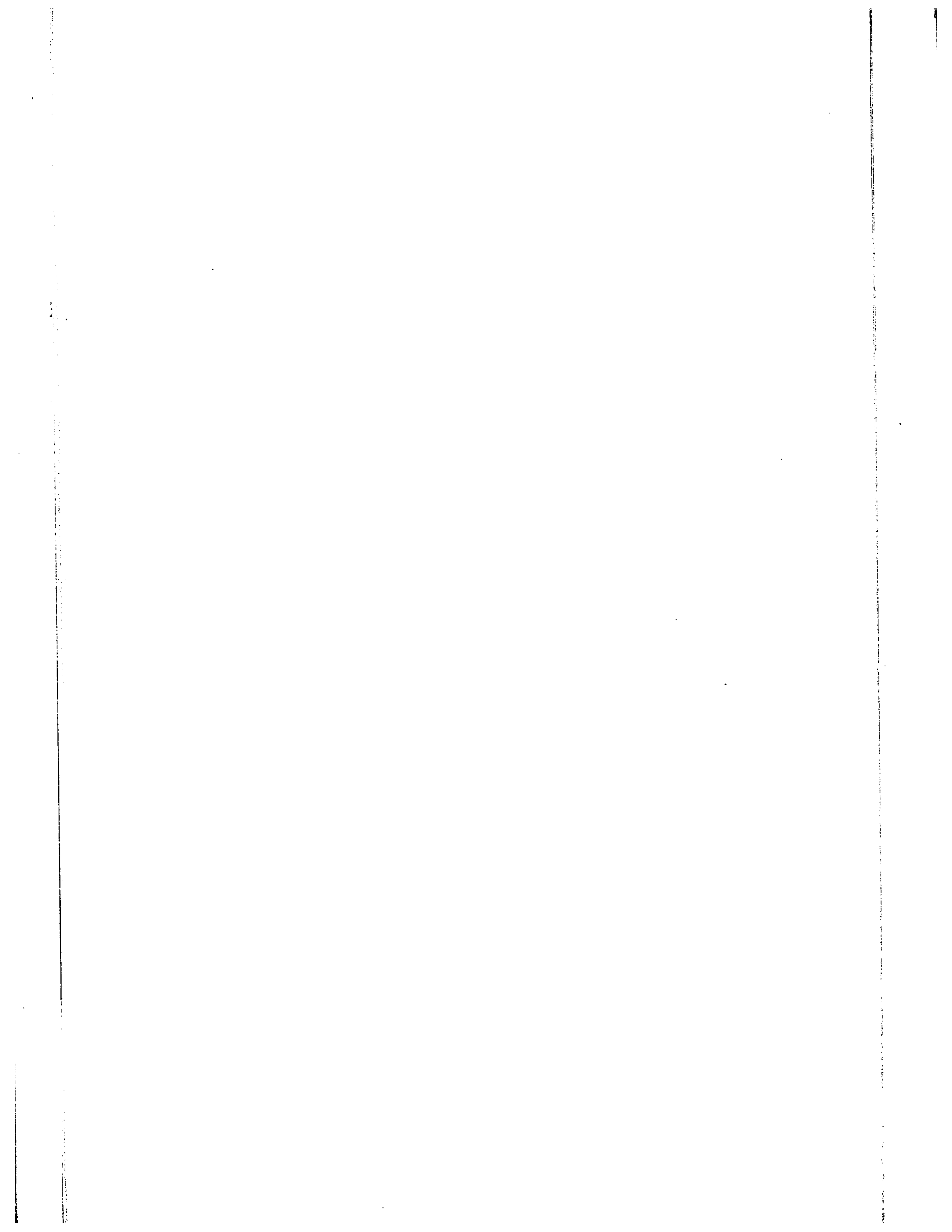

THE MULTIPURPOSE MICROELECTRONIC PROCESSOR

by

WINSTON R. SAMAROO

A thesis submitted in partial fulfilment
of the requirements for the degree of
Doctor of Philosophy

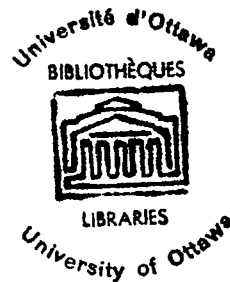

Department of Electrical Engineering
Faculty of Pure and Applied Science
The University of Ottawa
Ottawa, Canada

1965

UMI Number: DC52488

INFORMATION TO USERS

The quality of this reproduction is dependent upon the quality of the copy submitted. Broken or indistinct print, colored or poor quality illustrations and photographs, print bleed-through, substandard margins, and improper alignment can adversely affect reproduction.

In the unlikely event that the author did not send a complete manuscript and there are missing pages, these will be noted. Also, if unauthorized copyright material had to be removed, a note will indicate the deletion.

UMI®

UMI Microform DC52488
Copyright 2007 by ProQuest LLC
All rights reserved. This microform edition is protected against unauthorized copying under Title 17, United States Code.

ProQuest LLC
789 East Eisenhower Parkway
P.O. Box 1346
Ann Arbor, MI 48106-1346

I ABSTRACT

Since the inception of microelectronics only a few years ago, a number of techniques have been devised to solve some of the problems associated with the new concepts. The use of electron and ion-beam machines have led to some of the more important developments and the present trend indicates that these machines will shortly be standard equipment in the fabrication and study of microelectronic circuits.

This dissertation describes a microelectronic research facility, which integrates many of the processes required in the fabrication of microelectronic circuits and will, thereby, alleviate some of the basic difficulties arising from the small size of the circuit elements. The machine has been called the "Multipurpose Microelectronic Processor", which was abbreviated to MMP. The design of the MMP and the theory on which it is based have been fully discussed.

The MMP was designed primarily for basic research in microelectronics involving thin films but it will also permit the fabrication of microelectronic circuits and will facilitate research in related fields.

When completed, the MMP will permit controlled deposition of thin films from an ion beam, electron-beam micromachining, topological inspection using a scanning electron microscope, and chemical analysis using a micro-analyser. These processes will be achieved without the need of moving the substrate from one work station to another with the associated problems of reregistration and maintaining clean surfaces.

The vacuum system for the MMP has been completed and the scanning electron microscope is in operation. Some modifications to the main electron gun will be necessary to increase the resolution of the scanning electron microscope and to increase the beam power for the machining mode of the MMP.

The conditions from which the ideas for the design of the MMP arose are discussed in the Introduction.

In Chapter 1, the technology required in the fabrication of thin-film circuits is covered. Special attention is given to those processes, which are closely associated with the MMP.

A brief overall description of the MMP is given in Chapter 2.

In Chapter 3, two new mechanisms for the bending of ion beams are analysed and a practical design is presented for the ion beam deposition system in the MMP.

Chapters 4, 5 and 6 are devoted to the details and performance of the sub-systems in the MMP.

A concluding discussion is presented in Chapter 7.

II ACKNOWLEDGMENTS

I wish to express my appreciation to Professor G.S. Glinski for making it possible for me to work on the University of Ottawa Microelectronic Project. He suggested and supervised the work and I am thankful for his interest in those phases of the project in which I was involved.

I have found it a very pleasant experience working with Mr. T.J. Mousseau, the only other full-time employee on the microelectronic project. Without him, a project of this magnitude would not have been undertaken at the University.

Thanks are due to Dr. P. Savic of the National Research Council, to Dr. A. Gillison of the Department of Mines and Technical Surveys and to the members of the Departments of Electrical Engineering and Physics for their interesting discussions and useful suggestions. For the typing of the manuscript and her forbearance throughout this work, I thank my wife Louise.

The entire list of persons from whom services were received would be too long to mention. However, I would like to mention that Mr. T. Holtz of Mikros Inc. designed the electron lenses for the MMP and Miss O. Boshko wrote the digital computer program for the analysis of the ray equations.

The microelectronic project is sponsored by the National Research Council of Canada through Grant No. A-875

and the Defence Research Board of Canada through Grant No. 993-10, without which, this work would not have been possible.

III LIST OF SYMBOLS

$\dot{A}$	Angstroms, $1\ \dot{A} = 1 \times 10^{-10}$ metres.
B	Magnetic flux density in webers per square metre.
E	Electric field strength in volts per metre, $\tilde{E} = -\frac{dV}{dl}$.
e	Base of natural logarithms.
F	Force in newtons.
J	$\sqrt{-1}$.
k	Boltzmann's constant, $k = 1.38 \times 10^{-23}$ joules per degree.
M	Mass of a particle in kilograms.
q	Charge of a particle in coulombs.
T	Absolute temperature.
t	Time in seconds.
V	Potential in volts.
v	Velocity in metres per second.
$\dot{x}$	$\frac{dx}{dt}$, similarly for $\dot{y}$, $\dot{\theta}$ and $\dot{r}$.
$\ddot{x}$	$\frac{d^2x}{dt^2}$, similarly for $\ddot{y}$, $\ddot{\theta}$ and $\ddot{r}$.
ε	Dielectric const., for free space, $\varepsilon = 8.855 \times 10^{-12}$ farad/metre.
ϵ	Electronic charge, $\epsilon = -1.602 \times 10^{-19}$ coulombs.
η	Charge to mass ratio in coulombs per kilogram.
μ	Microns, $1\mu = 1 \times 10^{-6}$ metres.
μ_o	Permeability of free space, $\mu_o = 1.257 \times 10^{-6}$ henry/metre.
ϕ	Phase angle in radians.

ψ Magnetic flux in webers.

ω Angular frequency in radians per second.

ω_c Angular cyclotron frequency in radians per second.

V' $\frac{dV}{dz}$, similarly for r .

V'' $\frac{d^2V}{dz^2}$, similarly for r .

CONTENTS

I ABSTRACT I

II ACKNOWLEDGMENTS IV

III LIST OF SYMBOLS VI

INTRODUCTION 1

CHAPTER 1 THE TECHNOLOGY OF THIN-FILM CIRCUITRY 3

1.1 Deposition of Thin Films 5

1.1.1 Vacuum Evaporation 5

1.1.2 Cathodic Sputtering 6

1.1.3 Ion-Beam Deposition 6

1.1.4 Nucleation and Development 8

1.2 Pattern Generation 8

1.2.1 Selective Deposition 9

1.2.2 Photoetching 10

1.2.3 Electron-Beam Machining 10

1.2.4 Activated Electron - or Ion-Beam Machining 11

1.3 Circuit Inspection 12

1.3.1 Surface Inspection 13

1.3.2 Chemical Analysis 14

CHAPTER 2 THE MULTIPURPOSE MICROELECTRONIC PROCESSOR ... 16

CHAPTER 3 THE DEPOSITION SYSTEM 21

3.1 The Ion Source 23

3.2 Bending of the Ion Beam 24

3.3 The Bending Mechanism 24

3.3.1 Motion in the X-Y Plane 27

3.3.2 The Effect of Pulse Width 29

3.3.3 Motion in the Z-Direction 30

3.3.4 The Design of the Chamber 37

3.4 An Alternate Bending Mechanism 46

CHAPTER 4 THE MAIN ELECTRON BEAM AND MICROMACHINING 51

4.1 Requirements for Electron-Beam Micromachining 51

4.2 The Electron Optical Column 54

4.3 The Lens Assembly 54

4.4 The Electron Gun 56

4.5 The Deflection System 58

4.6 The Substrate Carrier and Stage 60

4.7 Power Supplies 66

4.8 Alignment of the Beam 68

4.9 Performance of the Machining Beam 70

CHAPTER 5 THE SCANNING ELECTRON MICROSCOPE AND MICROANALYSER 72

5.1 The Scanning System 76

5.2 The Electron Collector 77

5.2.1 The Photomultiplier, Cathode Follower and Preamplifier Assembly 78

	5.2.2	The Z-Axis Amplifier	80
	5.3	Intensity Modulation of the C.R.O. ...	80
	5.4	Performance of the Scanning Electron Microscope	81
	5.5	Provision for the Microanalyser	83
CHAPTER 6	THE VACUUM SYSTEM		84
	6.1	The High-Vacuum Assembly	85
	6.1.1	Vacuum Pumps	85
	6.1.2	Vacuum Gauges	87
	6.2	The Ultrahigh Vacuum	88
	6.3	Residual-Gas Analysis	89
	6.4	Leak Detection	89
	6.5	Protective Circuitry	90
	6.6	Performance of the Vacuum System	93
CHAPTER 7	DISCUSSION		99
	7.1	The Present State of the MMP	100
	7.2	Experimental-Research Projects	100
	7.2.1	The Preparation of Thin Films	101
	7.2.2	The Resolution of Micromachining	101
	7.2.3	The Fabrication of Thin-Film Circuits.	102
APPENDIX 1		....	103
APPENDIX 2		....	108
REFERENCES		....	110
VITA		....	114

INTRODUCTION

It will be shown in Chapter 1 that during the fabrication of a single thin-film circuit, a number of independent operations must be performed. Each operation lasts for only a short period, but the preparation for the operation may extend over a longer period, especially if the circuit is introduced into a vacuum system, which must then be pumped down from atmospheric pressure. To reduce the lost time between operations, some research workers (see reference 1) have interconnected as many as five vacuum chambers to form a sort of mechanized "in-line" processor. However, this does not solve all the problems associated with moving the substrate.

Each time the substrate upon which the circuit is being built is moved from one vacuum station to another, the problem of reregistration is introduced. Kenneth R. Shoulders (2) has calculated the feasibility of a computer, one inch cubed, containing 10^{11} components. Using a processor, which has more than one vacuum station (as is the case with Shoulders' system) to produce such a computer, would certainly involve considerable registration time.

The Multipurpose Microelectronic Processor (MMP)

is an experimental facility designed for research in microelectronics and for the fabrication of thin-film integrated circuits. Since flexibility was a keynote in the design of the MMP, the facility may also be used for research in many fields related to microelectronics. The MMP will permit the controlled deposition of thin films, electron-beam micromachining, topological inspection using a scanning electron microscope and chemical analysis using an electron-probe microanalyser. A complete work cycle consisting of any number of the above processes may be performed without interruption and with the original positioning of the substrate.

In Chapter 1, it will also be seen that some of the processes are performed under vacuum conditions, while others are performed in the laboratory atmosphere. This, of course, means that the film surfaces are subjected to contamination. In the MMP, such exposure is eliminated altogether.

Although the MMP will have some applications to the field of semiconductor integrated circuits, it is primarily concerned with thin-film circuitry. As a result, Chapter 1 is devoted to the technology of thin-film circuitry. This will form a basis for evaluating the approach taken to achieve the various processes in the MMP.

CHAPTER 1

THE TECHNOLOGY OF THIN-FILM CIRCUITRY

Thin-film integrated circuits are formed by one or more layers of thin films of conductors, semiconductors, dielectrics and ferromagnetic materials on a passive substrate. The substrate serves as a mechanical support for the rest of the circuit, therefore, it must be mechanically stable and chemically inert. It must have a low coefficient of expansion and the surface must be capable of a fine finish especially when very thin films are to be used. Most types of glass have been found suitable for use as substrates except those with a high soda content, where sodium ion migration causes deterioration of the circuit characteristics. Sapphire and glazed ceramics have also been used.

The metals commonly used in thin-film integrated circuits are tantalum, titanium, chromium, nickel and gold. Several other metals are used but to a lesser extent. Common dieletrics are tantalum pentoxide, aluminium oxide, titanium dioxide, silicon monoxide, and silicon dioxide. It is often advantageous to use metals such as tantalum and titanium since their oxides are good dielectrics.

Resistors are made by machining (see section 1.2.3) or etching around narrow strips of thin films. Resistors

are available from 10 to 500,000 ohms with a tolerance of about 2% and a resistance temperature coefficient of ± 0.03% per C°.

Capacitors are made by sandwiching a layer of dielectric between two layers of conductors. Capacitance values are available up to 10,000 picofarads with 10% stability and tolerance.

Large inductances cannot be built into small spaces, since large volumes are required for the storage of the energy associated with the large inductances. Inductors of about one microhenry have been made by spiralling a strip of thin conducting film, but inductances of this size are not very useful except at very high frequencies; and they occupy too large an area on the substrate. Inductors are replaced by active circuits wherever possible.

The outstanding drawback in the field of thin-film circuitry is the lack of a truly operative thin-film active device. However, research is being pursued in two areas: in thin-film transistors and in "hot-electron" devices.

Numerous ways of fabricating thin-film circuits have been used, but they all consist of a number of basic processes: i) the controlled deposition of thin films, ii) a method of pattern generation and iii) means for topological, chemical and electrical inspection.

1.1 Deposition of Thin Films

The usual methods of producing thin films in microelectronics are vacuum evaporation and cathodic sputtering. Ion-beam deposition, and "nucleation and development" are special methods which will eliminate much of the efforts currently spent on pattern generation (section 1.2). There are a number of other methods used to a lesser extent in microelectronics. These are described by L. Holland (3).

1.1.1 Vacuum Evaporation

In vacuum evaporation, the substrate is placed directly over a crucible containing the film material. The material is heated by any of several methods: joulian heating, induction heating or electron bombardment, and the evaporated material is deposited on the substrate. To reduce the loss of material through atomic or molecular collisions, the distance from the source to the substrate is made less than the atomic or molecular mean free path at the operating pressure. For most systems, a pressure of 10^{-3} torr (mm. of mercury pressure at $0^{o}C$) would satisfy this criterion; and the older vacuum evaporators operated with such pressures. The more modern systems now go as low as 10^{-9} torr in an effort to obtain high-purity films.

When joulian or induction heating is used, the films are contaminated with traces of the crucible material. By

using electron bombardment, the crucible may be dispensed with altogether. The electron beam is made to impinge on the top surface of the material specimen to maintain a molten pool, from which evaporation takes place. Electron bombardment also provides a higher intensity source and is more easily controlled than the other forms of heating.

1.1.2 Cathodic Sputtering

Recently, cathodic sputtering has become a very popular form of thin-film deposition. In cathodic sputtering, an arc discharge is passed between two sheet electrodes. In the discharge, cathode material is removed by inert-gas ion bombardment and is deposited on the substrate, which is positioned on the anode.

The mechanisms whereby cathodic sputtering takes place are reviewed by S.P. Wolksy (4) and techniques for the preparation of thin films for industrial use are covered by N. Schwartz (5). Schwartz treats reactive sputtering, whereby the properties of the sputtered films are varied by varying the reactive gas content of the sputtering atmosphere.

1.1.3 Ion-Beam Deposition

The deposition of thin films from an ion beam is still in the experimental stages. When perfected, this method of deposition will offer a number of advantages:

i) The possibility of selective deposition (see section 1.2.1). At present, selective deposition can only be achieved with fairly large dimensions through the use of masking techniques. Ion-beam deposition will allow the selective deposition of micron-sized components and will considerably reduce machining time.

ii) Features of complete automation. Since all the controls are electrical, complete automation is feasible with the associated reduction in production time and cost.

iii) Purification of the film material. The focusing apparatus of the ion beam may act as a mass selector with the result that the deposited films may be purer than the bulk material.

iv) Maintenance of a cleaner vacuum system. In vacuum evaporation, stray atoms or molecules are deposited anywhere in the vacuum system, while with an ion beam, strays are deposited on selected areas.

The requirements for an ion-beam deposition system are an ion source, a focusing system, a deflection system and control equipment. If selective deposition is not required (and this could always be added as the system is refined) the deflection system is omitted.

K. Norsworthy (6) of Boeing Corporation has recently reported the deposition of chromium resistors from an ion beam. The films showed a microcrystaline structure on

deposition, but recrystalization was possible using electron-beam heating.

1.1.4 Nucleation and Development

During nucleation, the surface energy of a specially prepared substrate is manipulated to form nucleation sites so that upon development, material is selectively deposited to form required patterns. Photography is a familiar example of this: after exposure, each grain of silver halide contains a few nuclei of silver, but on development, the entire grain of silver halide is converted to silver.

Nucleation may be achieved by the use of optical methods as in photography, electron bombardment or ion bombardment. Development may be done using molecular beams or vacuum evaporation.

Because the number of atoms or molecules present after development is considerably greater than the number before, Alfred F. and Erika E. Kaspaul (7) have termed the whole field "Molecular Amplification".

1.2 Pattern Generation

Once a thin film of material is deposited on the substrate, components, parts of components and interconnections must literally be carved from the film before another layer of different material is deposited. This layer may be carved and

another layer deposited until a circuit is built up. The carving process is referred to as pattern generation, which represents the most difficult step in the production of thin-film integrated circuits.

Pattern generation may be achieved by i) selective deposition, ii) photoetching, iii) electron-beam machining, iv) activated electron- or ion-beam machining.

1.2.1 Selective Deposition

In selective deposition, the material is deposited to form the required pattern thereby eliminating the need to generate the pattern at a later stage. It was already suggested that this may be accomplished through the use of ion-beam deposition or nucleation and development. These two methods are in the experimental stages. However, with suitable masking techniques and any of the standard deposition systems, thin films may be selectively deposited.

The preparation of a mask for deposition is laborious and unwieldly. The pattern is first drawn several times the required size so that accuracy may be obtained. From this drawing, a positive transparency is prepared by ordinary photographic means. A sheet of stainless steel, about 0.1mm. thick, is then coated with a photoresist emulsion and the emulsion is exposed by projecting a reduced image of the positive on it. After development, a negative of the pattern is obtained on the steel plate. The exposed parts

of the steel plate are etched away in a ferric chloride solution, the resist is dissolved in a solvent and the mask is ready for use.

Deposition through such masks produces lines accurate to about 2.5μ which is limited mainly by the etching process. The selective deposition of micron-sized elements, therefore, depends on the perfection of ion-beam deposition, and nucleation and development, which will have the required resolution.

1.2.2 Photoetching

If, during deposition, an entire surface of the substrate is covered with a thin film of material, photo-etching may be used to remove the unwanted parts of the film. The processes used here are almost exactly the same as those used in the production of masks.

The required pattern is drawn several times the desired size and a negative transparency is made. The thin film on the substrate is covered with a photoresist emulsion and a demagnified image of the negative is projected to expose the emulsion. After development, the bare portions of the film are removed by a suitable etchant.

1.2.3 Electron-Beam Machining

Within the past few years, electron beams have been

used as high powered sources in welding, smelting, melting, drilling and junction formation (alloying). An electron beam may be focused to a small spot concentrating powers up to 10^9 watts/cm^2 (8) which is sufficient to evaporate any known substance. Because of this, electron bombardment may be capable of the fine machining required to generate micron-sized components from thin films (see Chapter 4).

In electron-beam machining, it is desirable to provide a very intense source of heat to evaporate material without melting the surrounding region, since the area of the molten region is a determining factor in machining accuracy. For this reason, the electron beam is pulsed to allow the surrounding region to cool between pulses. K.H. Steigerwald (8) has calculated the pulsing technique to be valid and in his experimental work, has reported machined lines in silicon 3µ wide and 0.5µ deep.

G. Mollenstedt and R. Speidel (9) used a diaphragm to reduce their electron beam from 10µ to 100 Å and with the resulting beam irradiated a collodion foil to produce line widths of 140 Å. This is not machining but it is indicative of the possibilities for electron-beam micromachining.

1.2.4 Activated Electron- or Ion-Beam Machining

In the last section, the electron beam was used as a thermal source to evaporate unwanted material. In activated machining, the electron or ion beam is used mainly to bring about a chemical reaction.

Instead of using light to expose the photoresist emulsion in the production of resist layers, electrons with their shorter wavelengths and hence finer resolution, may be used. Resists produced in this manner give a resolution of 100 Å or less. A gaseous etchant is used with these resist layers, since a liquid etchant undercuts to a greater degree and destroys the resolution gained through the use of the electron beam.

Ion beams may also be used to expose photoresist emulsions but a more important use is as an etching beam. Ion beams of elements such as the halogens may be used to selectively etch thin films.

1.3 Circuit Inspection

One of the basic arguments for microelectronics is improved reliability and this has actually been proven with the present generation of circuits (10, 11). Microelectronic circuits are so reliable that once they have reached the production stage, the testing of individual circuits is hardly necessary.

It is in the research and development stages that close inspection is required. For relatively large circuits, a high powered microscope and a few electrical jigs are all that is required. For research into the physical properties of very thin films and investigation of unknown molecular phenomena, however, elaborate equipment must be provided for inspection.

1.3.1 Surface Inspection

For the surface inspection of micron-sized thin-film components, some form of electron microscope is desirable, because of its high resolution. The transmission electron microscope, which has a resolution of a few Angstroms, is not very useful because the substrate upon which the thin films are deposited is generally too thick for the transmission of electrons. Obtaining a replica of the surface for viewing on the transmission instrument is cumbersome and time-consuming. Therefore, other types of electron microscopes are better suited for this purpose.

In the reflection electron microscope, primary electrons are directed to the surface to be examined and the back-scattered electrons are focused by lenses to form an image of the surface. The resolution of these instruments is about a few hundred Angstroms.

An instrument which is very useful in surface inspection is the scanning electron microscope. This instrument is sometimes included in the class of electron emission microscopes, although it does not actually belong there. In the electron emission microscope, the specimen is made to emit electrons either by heating, photoemission or electron bombardment and the electrons are accelerated and focused to form an image.

In the scanning electron microscope, the final image is not due to the focusing of the emitted electrons. A finely focused electron beam or probe is scanned over the

specimen in a television-like fashion and the emitted secondary electrons are collected and used to intensity modulate a CRT scanning in synchronism with the electron probe. A magnified image of the scanned object therefore appears on the face of the CRT. The resolution of this instrument is approximately equal to the probe diameter, which may be less than 100 Å. Although secondary electrons were specifically mentioned, reflected (backscattered) electrons may be used in a similar fashion.

1.3.2 Chemical Analysis

When experimenting with thin-film elements with surface dimensions of the order of a micron, it is often necessary to know the purity of the film material and the type of impurities present. During deposition, a mass spectrometer may be used to analyse samples of the material being deposited, but for non-destructive analysis of small areas of thin films, the electron-probe microanalyser is a desirable instrument.

The microanalyser uses an electron probe similar to that used in the scanning electron microscope. The more exact method of using the microanalyser is to focus the probe on the chosen spot on the specimen and analyse the emitted x-rays using a suitable spectrometer. From measurements of the wavelength and intensity of the x-rays, the elements and their mass concentration may be determined. Another method

is to use the reflected electrons to form an image as is done in the scanning electron microscope. S. Kimoto and H. Hashimoto (12) have shown that either the image due to variations in chemical composition or the image due to surface topography may be obtained. This is done by either adding or subtracting the outputs from a pair of matched electron collectors placed opposite each other.

CHAPTER 2

THE MULTIPURPOSE MICROELECTRONIC PROCESSOR

A photograph of the MMP without the control and display units is shown in Figure 1. In Figure 2, the bell-jar has been removed to expose the part of the electron optical column which extends above the baseplate. The lower part of this column can be seen in both Figures 1 and 2.

A diagram of the internal structure of the MMP is shown in Figure 3. At the top of the electron optical column is the stage, 2, 3 and 4, with the substrate carrier, 1.

At the lower end of the optical column is the main electron gun 12, 13 and 14. The electron beam produced by this gun will be used for machining and under reduced power, it will be used to form the probe for the scanning electron microscope and the microanalyser.

Since machining, scanning electron microscopy and microanalysis require a high resolution, the axis normal to the substrate is reserved for the electron beam used in these processes. Thin-film deposition is accomplished through an ion beam, which is bent to meet the axis normal to the substrate. The ion source is, therefore, placed off the main axis of the instrument as shown in Figure 3.

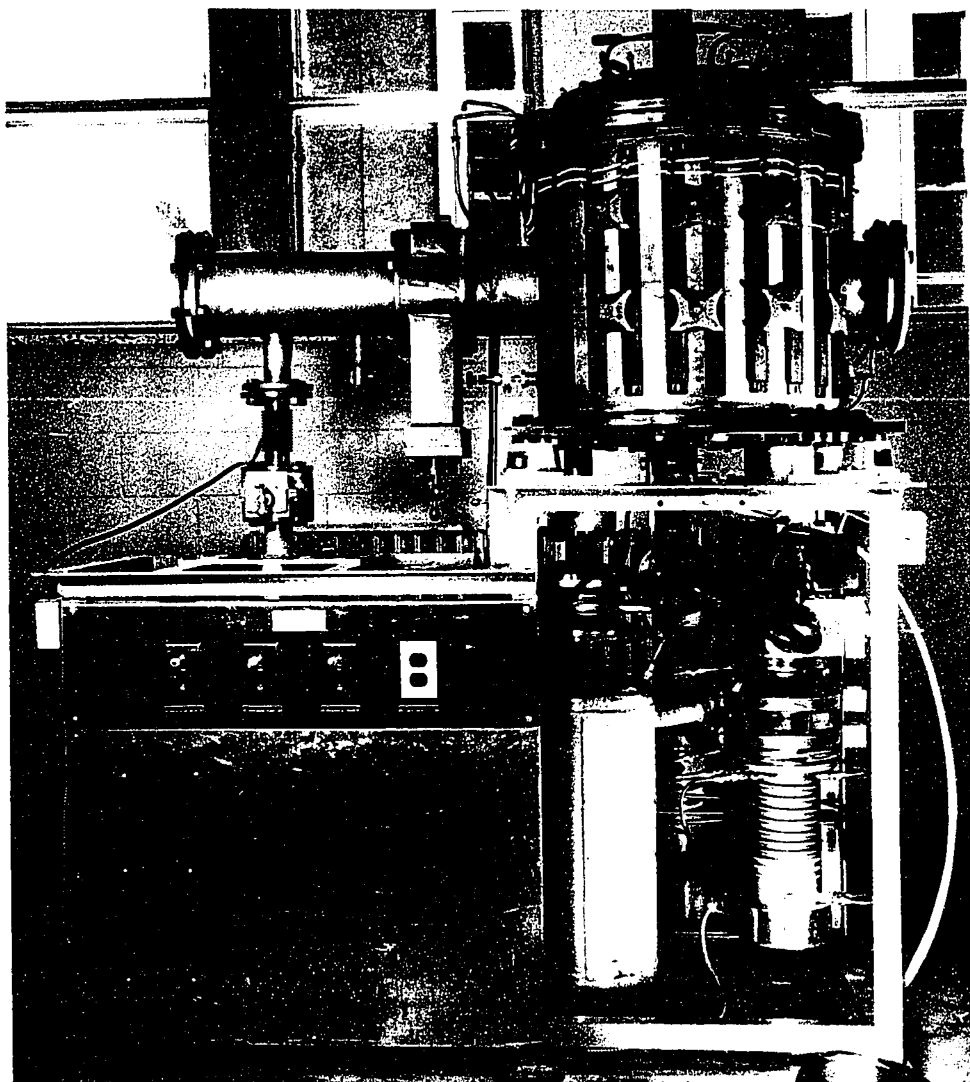

FIGURE 1

The Multipurpose Microelectronic Processor

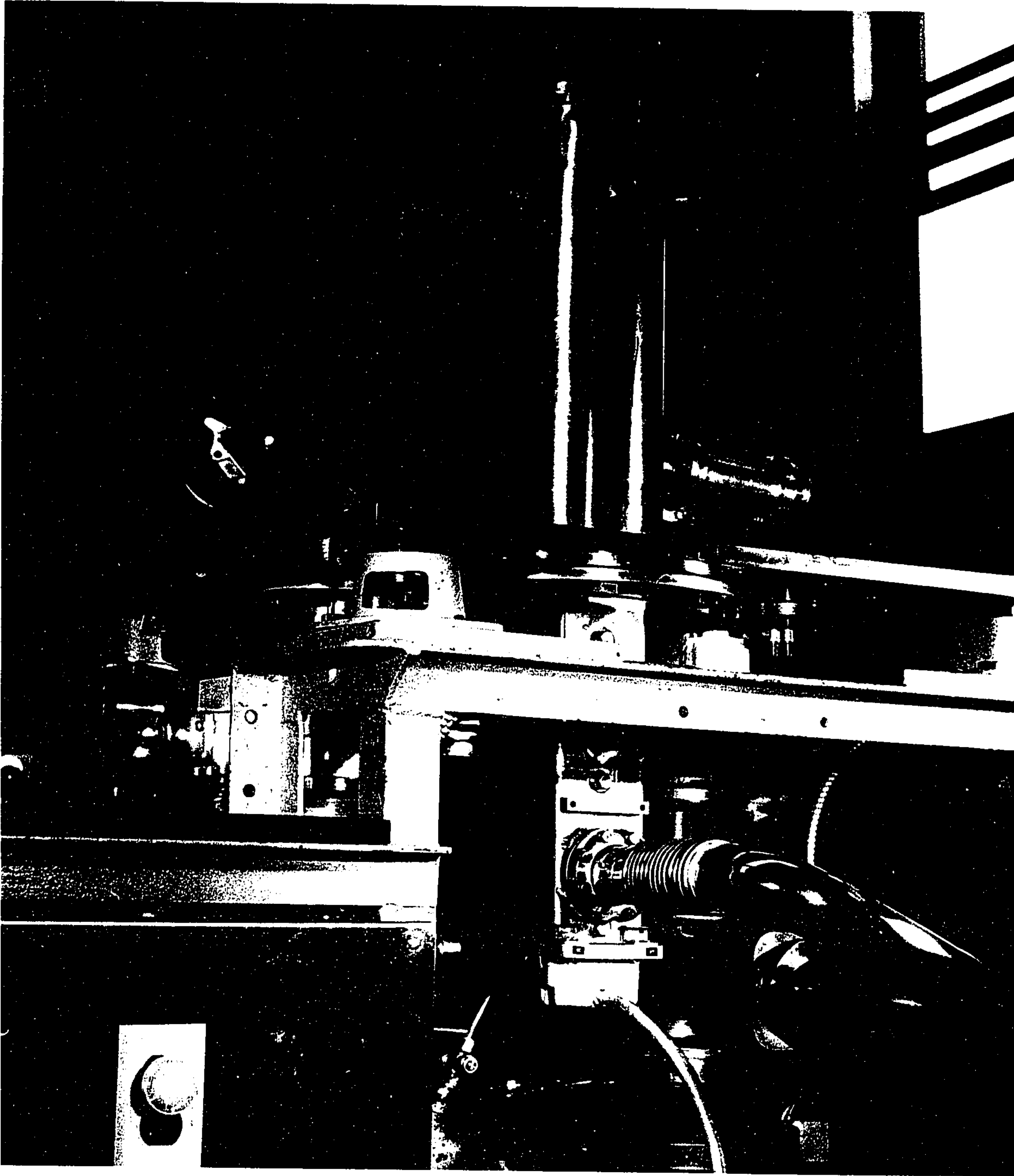

FIGURE 2

The Multipurpose Microelectronic Processor
with the belljar removed

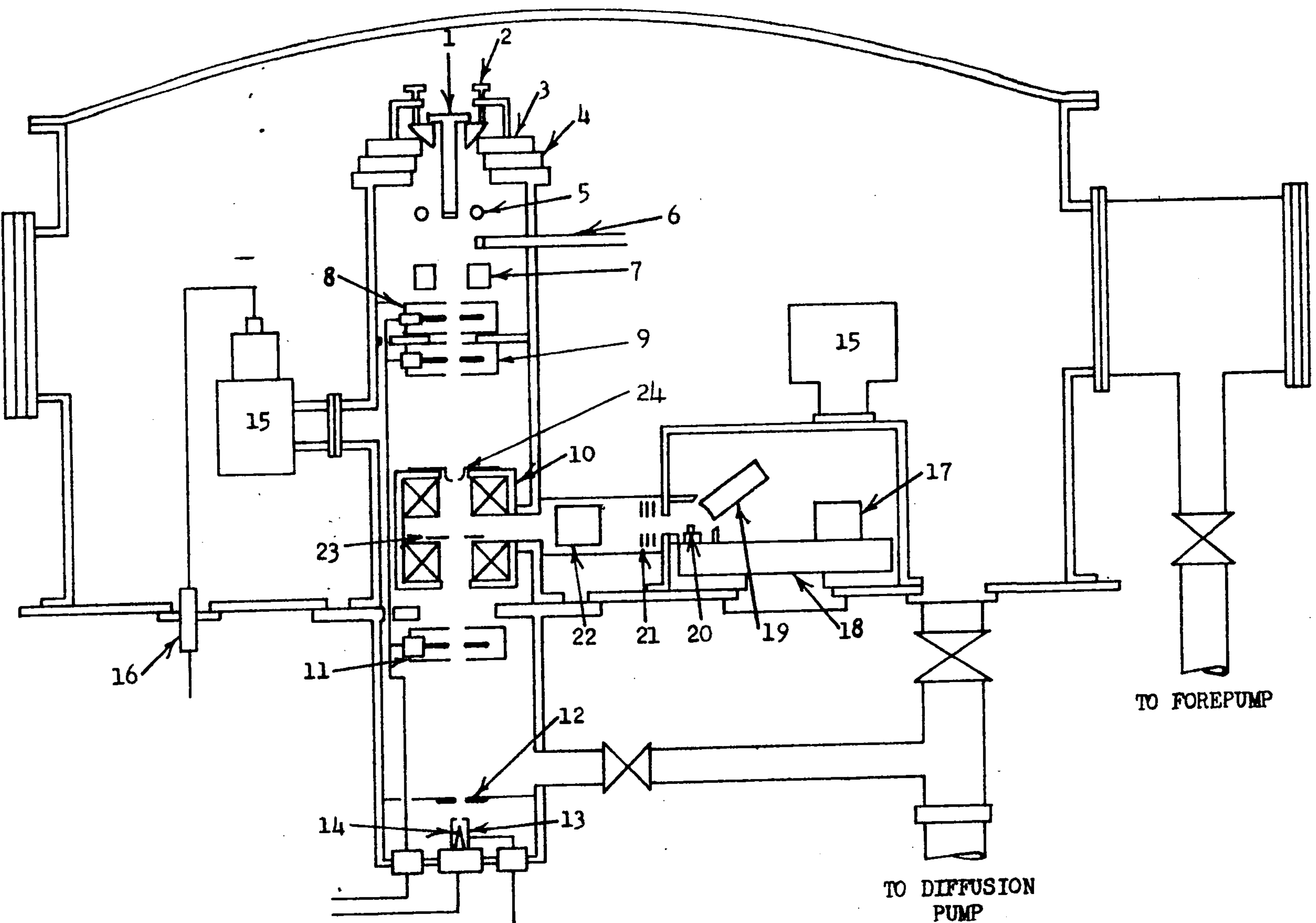

FIGURE 3

1. Substrate carrier, 2. Tilt adjust, 3. X-translation, 4. Y-translation, 5. Neutralization electrode, 6. Light piping, 7. Deflection plates, 8. Second electron lens, 9. Ion lens, 10. Magnetic chamber, 11. First electron lens, 12. Anode, 13. Wehnelt cap, 14. Filament, 15. Ion pump, 16. Feedthroughs, 17. Turntable drive, 18. Turntable, 19. Pierce gun, 20. Thin-film material, 21. Extraction electrodes, 22. Ion optics, 23. Accelerator electrode, 24. Hemispherical electrode.

In the MMP, two stages of vacuum are used. The upper electron optical column which contains the substrate is evacuated to an ultrahigh vacuum of 1×10^{-9} torr. Because of the numerous seals in the stage which allows the substrate to be tilted, rotated, and translated in the x and y directions, a high vacuum region of 2×10^{-7} torr surrounds the ultrahigh vacuum region.

Chapters 3, 4, 5 and 6 treat in more details the component parts of the MMP.

CHAPTER 3

THE DEPOSITION SYSTEM

An ion-beam deposition system was chosen for the MMP in the hope that selective deposition will be achieved at some later date. Initially, the entire surface of the substrate will be covered by the deposited material and electron-beam micromachining will be used to generate the components and interconnections. Ion-beam deposition was also chosen because it will allow the source material, together with the associated equipment, to be placed away from the main axis of the equipment.

Figure 4 shows a diagram of the deposition system. Ions produced at the source are focused by the extraction electrodes into the magnetic chamber. Here the ion beam changes direction (see section 3.3) and leaves through the hemispherical electrode. The electrostatic ion lens focuses the ions to a spot at the substrate. The annular neutralization electrode is at ground potential and emits electrons, which will reduce charge build-up on the substrate. Neutralization of charge build-up on the substrate is desirable to reduce the divergence of the ion beam before it meets the substrate.

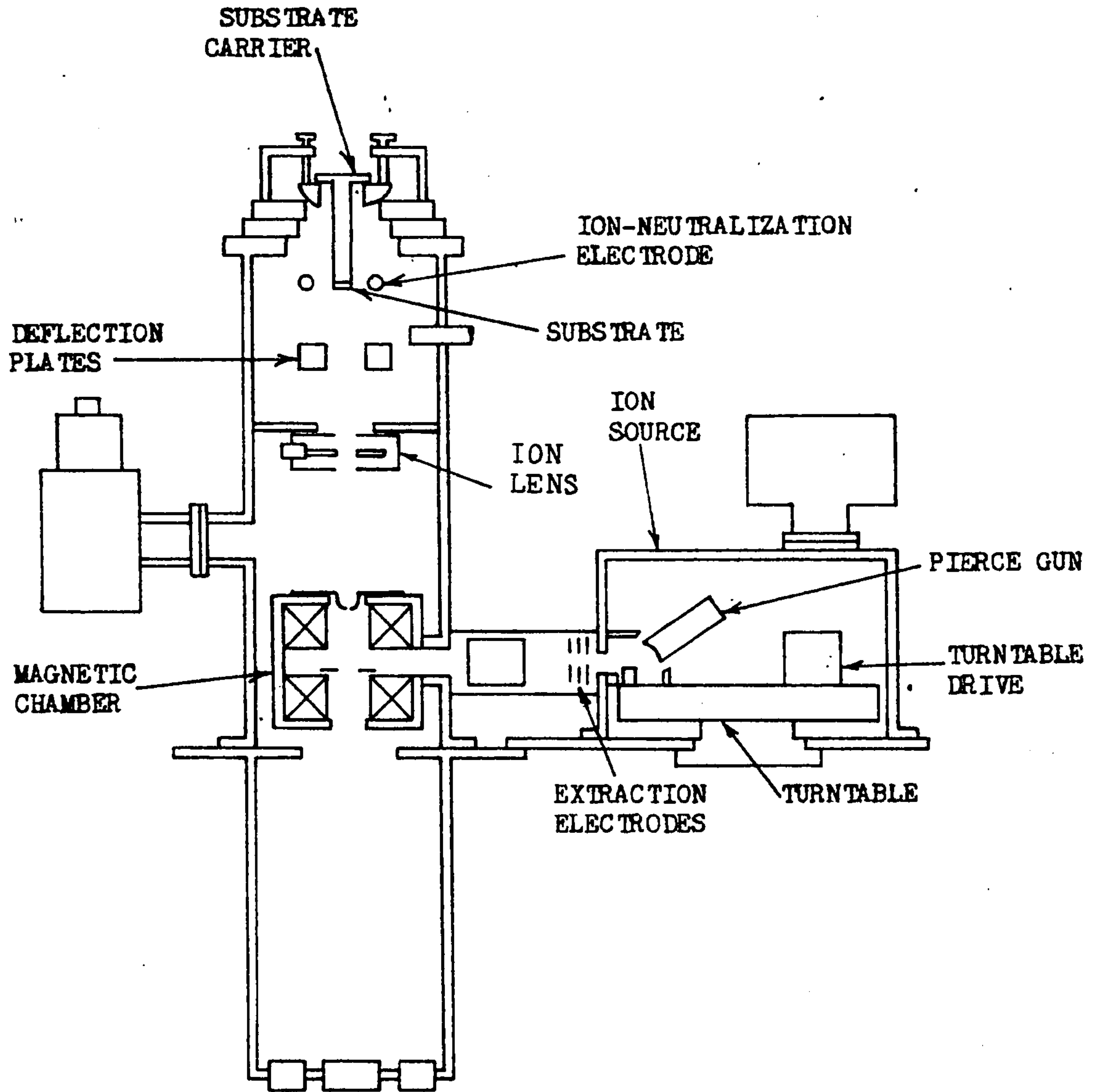

FIGURE 4

The deposition system

Dielectrics such as tantalum pentoxide, titanium dioxide, and alumina will be deposited from an ion beam of the corresponding metal in a partial pressure of oxygen (13).

3.1 The Ion Source

The original design of the ion source is shown in Figure 4. The materials to be deposited are stored on platens around the periphery of the turntable so that selected materials may be rotated into position at the focus of the ionizing gun. The ionizing gun is a Pierce gun in pulsed operation, since a pulsed beam rather than a continuous one results in a better efficiency for processes such as evaporation and ionization (14).

The proposed ion source has not as yet been built but the MMP provides sufficient flexibility so that any type of ion source may be coupled to the system.

At Cornell Aeronautical Laboratory, 1 amp of ions and 100 amps of electrons were obtained from a 0.020 inch diameter wire radiated with 6 watts of focused light from a laser (15). Such a system may prove to be a better ionization source for the MMP. GaAs p-n junction injection lasers are available with a power rating of 10 watts in pulsed operation (16).

3.2 The Bending of the Ion Beam

A system used in many instruments for bending beams of charged particles is a uniform magnetic field perpendicular to the beam. This system gives a line focus and is, therefore, unsuitable for the ion beam if selective deposition is to be achieved. For selective deposition, a spot focus is required at the substrate.

Two other systems for bending the ion beam are analysed theoretically and for the system chosen, a practical design is presented. Section 3.3 treats the chosen system, which consists of a uniform magnetic field and a crossed rotating electric field. The alternate method consists of a magnetic hump in space and is treated in section 3.4. Actually the rotating electric field system was developed to alleviate some difficulties encountered in the magnetic hump method.

3.3 The Bending Mechanism

Figure 5 shows the magnetic chamber in which the ion beam is bent, Figure 6 shows the system of fields existing within the chamber and Figure 7 shows a cross-section. Four vertical plates are used to produce the electric field rotating in the x-y plane and two aiding water-cooled solenoids produce a uniform magnetic field pointing in the z-direction. The electric field accelerating the ions in the z-direction will be discussed in section 3.3.3.

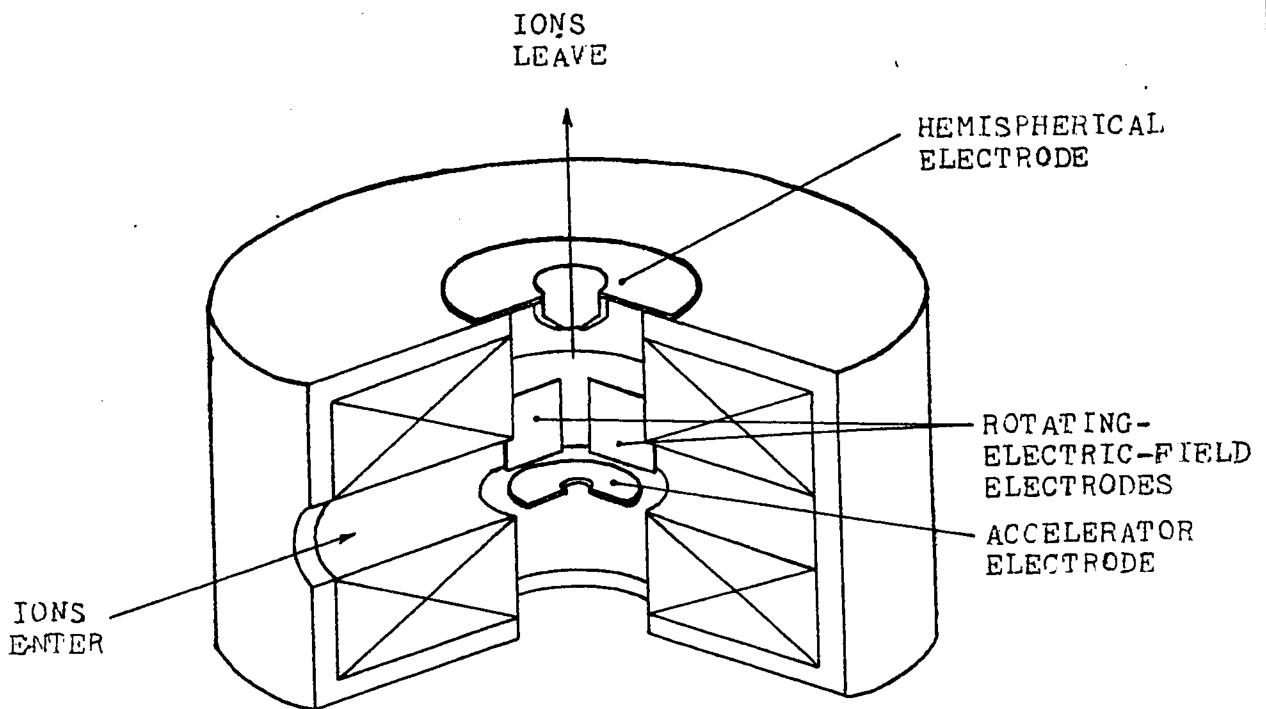

FIGURE 5

Details of the magnetic chamber

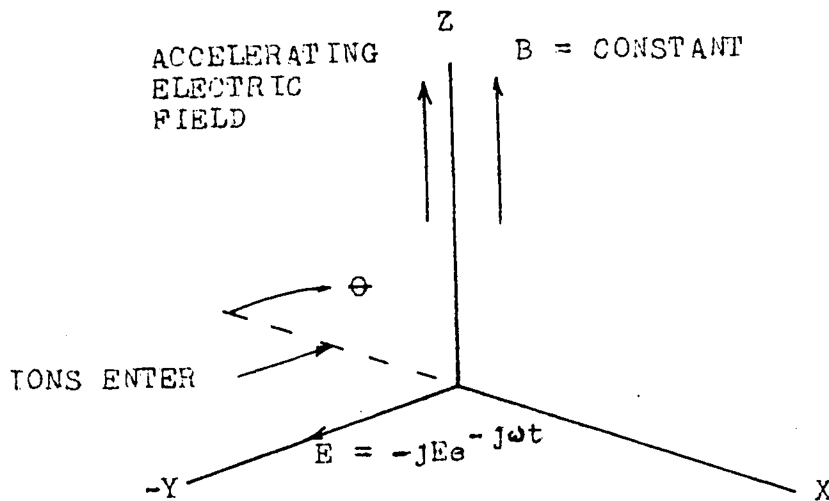

FIGURE 6

System of fields within the magnetic chamber

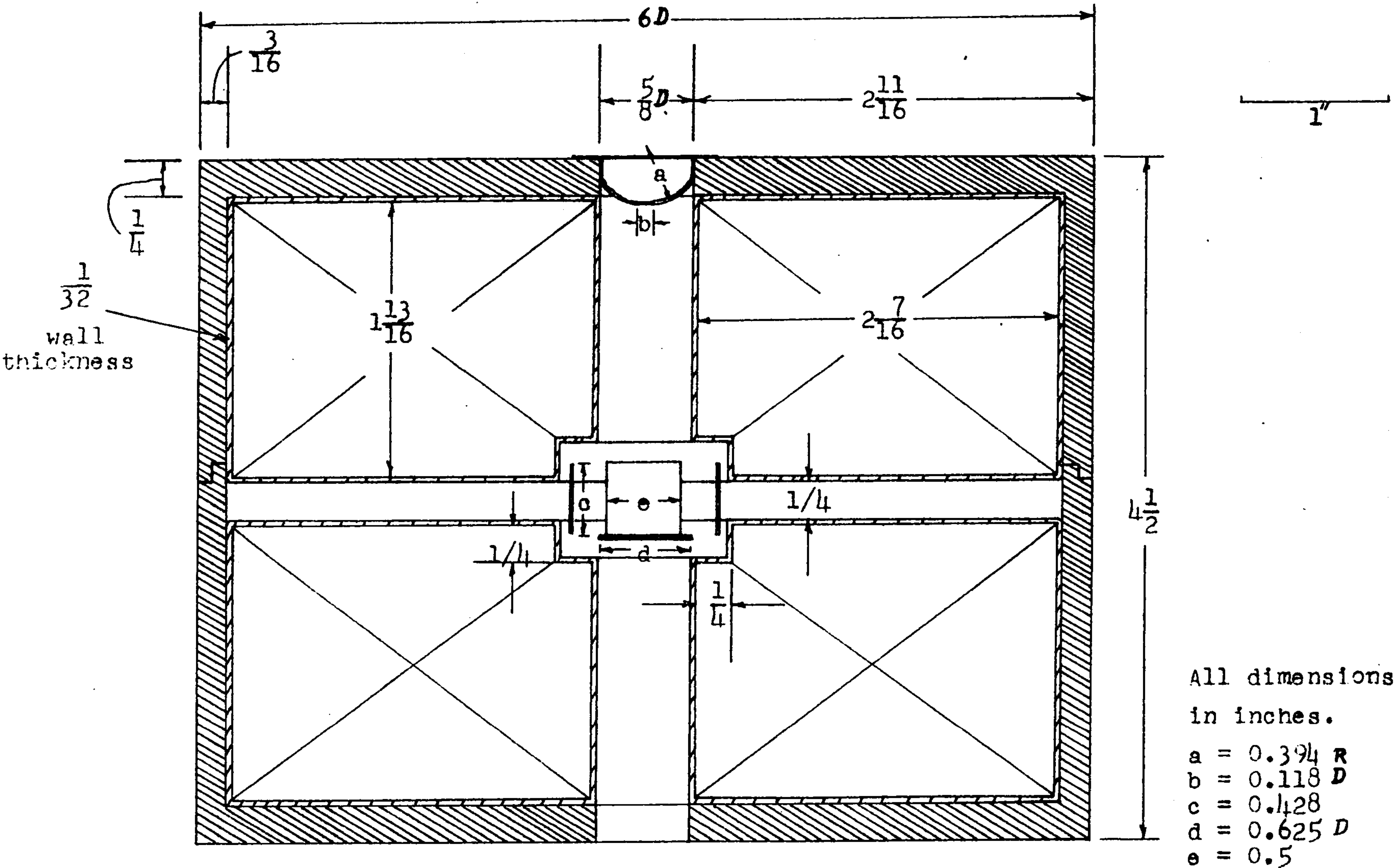

FIGURE 7

Cross section of the magnetic chamber

Ions are injected into the system of fields perpendicular to the z-axis, at a distance r_o from the origin. Under certain conditions, which will be discussed, the ions gyrate around the z-axis with decreasing radii. Eventually, their radii begin to increase again, but the ions are accelerated axially out of the rotating electric field before this happens. The shape of the field accelerating the ions in the z-direction is such that focusing takes place and the ions leave the magnetic chamber with a spot focus.

3.3.1 Motion in the X-Y Plane

Ions are injected into the system of fields, in which the angular frequency, ω, of the rotating electric field is equal to the angular cyclotron frequency, $\omega_c = \eta B$, where η is the charge to mass ratio in coulombs per kilogram and B is the magnetic flux density in webers per square metre.

The forces acting on an ion are the Lorentz force and the electric force, therefore,

$$F_x = M\ddot{x} = q\dot{y}B + qE_x \qquad (1)$$

$$F_y = M\ddot{y} = -q\dot{x}B + qE_y \qquad (2)$$

Replacing $\frac{q}{M}$ by η, ηB by ω, E_x by $-E \sin \omega t$ and E_y by $-E \cos \omega t$, equations (1) and (2) may be rewritten

$$\ddot{x} = \omega\dot{y} - \eta E \sin \omega t \tag{3}$$

$$\ddot{y} = -\omega\dot{x} - \eta E \cos \omega t \tag{4}$$

If at t = 0, the ion were injected into the system of fields at $x = -r_o$ and $y = 0$, with an initial velocity $\dot{y} = \omega r_o$, the ion will attain an initial velocity $\dot{x} = \frac{\eta E}{\omega}$ due to the drift caused by the crossed electric and magnetic fields. Under these initial conditions, the solution to equations (3) and (4) is

$$x = (-r_o + \frac{\eta E}{\omega} t) \cos \omega t \tag{5}$$

$$y = (r_o - \frac{\eta E}{\omega} t) \sin \omega t \tag{6}$$

combined to give

$$r = \left| r_o - \frac{\eta E}{\omega} t \right| \tag{7}$$

or

$$r = \left| r_o - \frac{E}{B} t \right| \tag{8}$$

The electric field $\overline{E}$ is at all times perpendicular to $\overline{r}$ and it is the drift caused by the crossed electric and magnetic fields, that gives the radial velocity indicated by the last term in equation (8).

Equation (8) shows that the ion spirals towards the centre of the chamber, achieves zero radius and then spirals out. If the ion is accelerated in the z-direction so that it leaves the rotating electric field when the radius is about zero, the trajectory of the ion would have been bent through 90°.

The motion of the ions in the x-y plane brings to mind the reversed trajectory of a charged particle in a cyclotron. However, both the mechanism and the results are sufficiently different so as not to warrant a detailed comparison.

3.3.2 The Effect of Pulse Width

Equation (8) was derived for the case where the radius vector $\overline{r}$ led the field $\overline{E}$ by exactly $\frac{\pi}{2}$ radians. In a pulsed beam, this angle will vary for each ion and will lie somewhere between $\frac{\pi}{2} - \phi_1$ and $\frac{\pi}{2} + \phi_2$, where $\frac{\phi_1 + \phi_2}{2\pi}$ is the ratio of the pulse width to the period of the pulse.

For any ion in the pulse, equations (3) and (4) may be rewritten as

$$\ddot{x} = \omega\dot{y} - \eta E \operatorname{Sin}(\omega t \pm \phi) \tag{9}$$

$$\ddot{y} = -\omega\dot{x} - \eta E \operatorname{Cos}(\omega t \pm \phi) \tag{10}$$

Where $0 \leqslant |\phi| \leqslant$ the larger of $|\phi_1|$ or $|\phi_2|$. So far, no restriction has been placed on ϕ, since in the limit $\phi_1 = \phi_2 = \pi$ and a continuous beam results. At $t = 0$, the time when the ion enters the system, $x = - r_o$, $y = 0$, $\dot{x} = \frac{\eta E}{\omega} \operatorname{Cos} \phi$ and $\dot{y} = \omega r_o \mp \frac{\eta E}{\omega} \operatorname{Sin} \phi$; and the solution to (9) and (10) is

$$x = - r_o \operatorname{Cos} \omega t + \frac{\eta E t}{\omega} \operatorname{Cos}(\omega t \pm \phi)$$

$$y = r_o \operatorname{Sin} \omega t - \frac{\eta E t}{\omega} \operatorname{Sin}(\omega t \pm \phi)$$

Combined to give

$$r^2 = r_o^2 + \left(\frac{\eta E t}{\omega}\right)^2 - \frac{2\eta E r_o t}{\omega} \cos\phi \qquad (11)$$

This shows that for $0 \leqslant |\phi| \leqslant \frac{\pi}{2}$, r decreases and for $\frac{\pi}{2} \leqslant |\phi| \leqslant \pi$, r increases. Also from equation (11), a minimum radius will be found to occur at a time, t_m, given by

$$t_m = \frac{\omega r_o}{\eta E} \cos\phi \qquad (12)$$

which when substituted back into (11) gives the minimum radius

$$r_m = r_o \sin\phi \qquad (13)$$

Therefore, ϕ should be restricted to small angles. In addition, from section 3.1, $\frac{\phi_1 + \phi_2}{2\pi}$ should be small, of the order of 1×10^{-2} (17), for a high efficiency ion source. Using such a ratio, for example, and assuming $\phi_1 = \phi_2$, the minimum radius achievable for the ions at the edges of the pulse will be $0.03\, r_o$. As the position of the ions tends towards the centre of the pulse, r_m tends to zero.

The effect of ions injected into the system at $r = r_o \pm \Delta r$ will be discussed in section 3.3.3.

3.3.3 Motion in the Z-Direction

So far, it was assumed that any motion in the x-y plane was independent of the electric field accelerating the ions in the z-direction. As shown in Figure 5, this field is produced by a hemispherical electrode at ground potential

and a flat accelerator electrode at a high positive potential. If the potential on the accelerator electrode is taken as zero reference, then the potential along the z-axis may be represented by

$$V_{(z)} = -\frac{2Az}{L^2-z^2} \tag{14}$$

where L is the distance from the accelerator electrode to the centre of the hemispherical electrode. A is a constant which is determined by specifying that the potential of the surface of the hemispherical electrode of radius "a" is V_1. Therefore,

$$A = -\frac{a(2L-a)V_1}{2(L-a)} \tag{15}$$

From equation (14) and Laplace's equation, the axially symmetrical field V(z,r) is found to be

$$V(z,r) = A\left[\frac{1}{\sqrt{(L+z)^2+r^2}} - \frac{1}{\sqrt{(L-z)^2+r^2}}\right] \tag{16}$$

a plot of which is shown in Figure 8.

Equation (16) describes exactly the potential field due to two isolated point charges, + A and - A, separated by a distance 2L, z being measured from the mid-point of the line joining the two charges in the direction of the negative charge. In the magnetic chamber, equation (16) will be a good representation of the field close to the z-axis. Further away, the magnet coil will affect the field. Another source of discrepancy will be the aperture in the hemispherical electrode. However, this may be corrected by the addition of

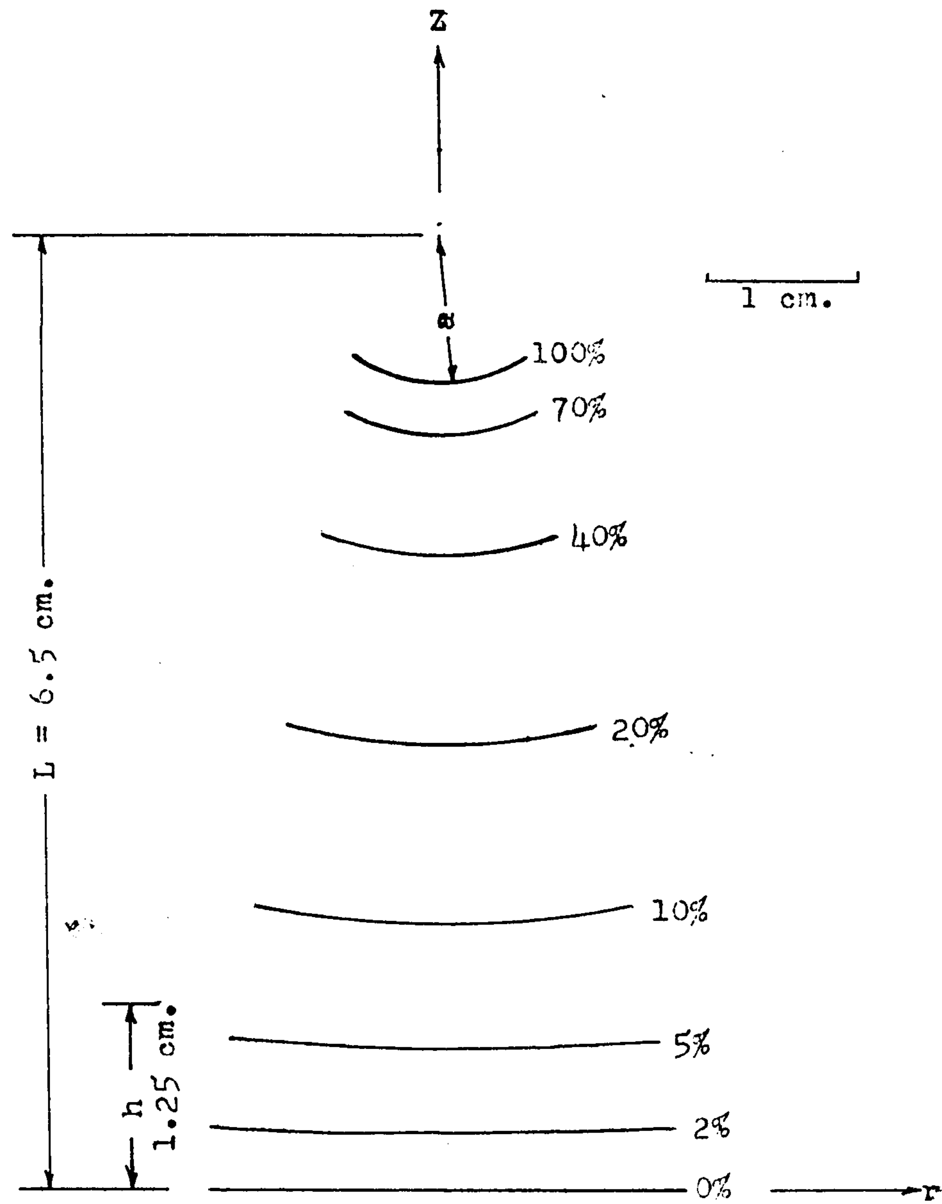

FIGURE 8

Plot of V(z,r) for L = 6.5 cm. and a = 1.0 cm. with the height of the rotating-electric-field electrodes, h, shown

other electrodes, the shapes and potentials of which are best determined experimentally.

The equipotential surfaces close to the accelerator electrode are almost flat. If this flatness is assumed to extend the length of the rotating-electric-field electrodes, then motion in the x-y plane as treated in sections 3.3.1 and 3.3.2 is independent of the electric field which accelerates the ions in the z-direction.

The space extending in the z-direction will be divided into three regions: Region I which is within the rotating-electric-field electrodes, Region II which is above the rotating-electric-field electrodes but within the magnetic chamber and Region III which is outside the magnetic chamber.

For convenience, a ray equation for Region II will be derived first. In this region, the ions are in a uniform magnetic field and the electric potential field V(z,r). The radial force on an ion is, therefore,

$$F_r = M(\ddot{r} - r\,\dot{\theta}^2) \tag{17}$$

from which

$$\ddot{r} - r\dot{\theta}^2 = -\frac{\eta\,\delta V(z,r)}{\delta r} - \eta r\dot{\theta}B \tag{18}$$

From Busch's theorem (18)

$$\frac{\eta}{2\pi}\, d\psi = d(r^2\dot{\theta}) \tag{19}$$

where ψ is given by

$$\psi = 2\pi\int_0^r B_z\, r\, dr \tag{20}$$

For a uniform magnetic field and an initial angular velocity, $\dot{\theta}_1 = \eta B$, at $z = z_1$ and $r = r_1$, equation (19) yields

$$\dot{\theta} = \frac{\eta B}{2} \left(1 + \frac{r_1^2}{r^2}\right) \tag{21}$$

and, therefore,

$$\dot{\theta}^2 = \frac{\eta^2 B^2}{4} \left(1 + \frac{r_1^2}{r^2}\right)^2 \tag{22}$$

An expression for $V(z,r)$ in terms of $V(z)$ and its derivatives with respect to z may be obtained by expanding $V(z,r)$ in a power series; neglecting terms with odd powers of r, since the axially symmetrical potential does not depend on the sign of r; performing the operations required by the two terms of Laplace's equation for an axially symmetrical field; and equating the coefficients for all powers of r to zero (19). Neglecting higher order terms,

$$V(z,r) = V - \frac{1}{4} V'' r^2 \tag{23}$$

where V represents $V(z)$ and V'' is the second derivative of $V(z)$ with respect to z. Similarly, V', which will shortly be used, is the first derivative of $V(z)$ with respect to z. These notations will be used throughout the rest of this section and the next. From equation (23),

$$\frac{\delta V(z,r)}{\delta r} = -\frac{1}{2} V'' r \tag{24}$$

Equation (24) was derived from Laplace's equation

and, therefore, if space charge is to be taken into consideration, the radial electric field due to space charge must be added to equation (24).

Assuming that the pulses of ions are cylinders of uniform charge distribution, Gauss's law may be used to find the radial electric field. Neglecting the end surfaces of the pulse, this gives

$$E_r = \frac{\rho r}{2\varepsilon} = -\frac{\delta V_s}{\delta r} \tag{25}$$

where ρ is the space charge density and is given by

$$\rho = \frac{I}{\pi r^2 \dot{z}} = \frac{I}{\pi r^2 \sqrt{2\eta |V|}} \tag{26}$$

I is the current in amps enclosed by an ion path at r. Substituting in equation (24)

$$\frac{\delta V(z,r)}{\delta r} = -\frac{1}{2}\left(V'' + \frac{I}{\pi r^2 \varepsilon \sqrt{2\eta |V|}}\right) r \tag{27}$$

The derivatives of r with respect to t will now be expressed in terms of derivatives with respect to z.

$$\dot{r} = r' \dot{z} \tag{28}$$

$$\ddot{r} = r'' \dot{z}^2 + r' \ddot{z} \tag{29}$$

$$\dot{z}^2 = 2\eta |V| \tag{30}$$

$$\ddot{z} = -\eta V' \tag{31}$$

Therefore,

$$\ddot{r} = 2\eta |V| r'' - \eta V' r' \tag{32}$$

Substituting equations (21), (22), (27) and (32)

into (18) gives

$$r'' + \frac{V'}{2V} r' + \left(\frac{V''}{4V} - \frac{\eta B^2}{8V} \right) r + \frac{I}{4\pi \mathcal{E} (2\eta |V|)^{1/2} V} \frac{1}{r} + \frac{\eta B^2 r_1^4}{8V} \frac{1}{r^3} = 0 \tag{33}$$

Equation (33) gives the trajectories of ions close to the axis and enclosing a current I.

In Region I, there is no true axis of symmetry although the z-axis of the rectangular coordinate system used in sections 3.3.1 and 3.3.2 was made to coincide with the axis of symmetry of Region II. For ions injected into the system at $r = r_o \pm \Delta r$, equations (9) and (10) are still applicable by shifting the origin of the rectangular coordinate system by $\pm \Delta r$. This effect combined with the acceleration due to the field in the z-direction will, therefore, give an ion image of radius $r_m + \Delta r$ at $z = z_1$, the boundary between Regions I and II.

The effect of space charge on the image size at $z = z_1$ may be calculated by finding the beam spread about the trajectory of an ion from the centre of the pulse. The interaction between the electric field due to space charge and other fields is assumed to be of second order and the velocity of the ions is the vector sum of the velocities in the x-y plane and the z-direction, which is nowhere equal to zero.

However, a virtual image of radius $r_m + \Delta r$ exists

at $z = 0$ and, therefore, equation (33) may be extended to Region I. In this case, the virtual path of the ions is shorter than the actual path but the velocity of the ions does start at zero.

B was specified to be constant in Regions I and II. It will now be assumed that the transition region where B drops to zero is short in comparison to the length L and that this transition takes place at the boundary of Regions II and III. Region III is, therefore, field-free space and equation (33) reduces to

$$r'' - \frac{I}{4\pi\varepsilon(2\eta)^{1/2}\,|V_1|^{3/2}}\,\frac{1}{r} = 0 \qquad (34)$$

where the beam voltage is now the constant value, $-V_1$.

The ray equations derived in this section will be further discussed in section 3.3.4, and a numerical analysis will be presented for the design values.

3.3.4 The Design of the Chamber

Among the materials to be deposited, tantalum presents the most difficulty because of its large atomic mass. For example, the velocity with which the ions are injected into the system is given by

$$v_h = \eta B r_o \qquad (35)$$

Since η for tantalum is low, B must be high to allow for

practical values of v_h. It is easier to control the beam characteristics at the entrance to the system if v_h is not too close to zero.

For a given beam voltage, the space charge effect will be most significant for tantalum, again because of its low η.

The system will, therefore, be designed for tantalum and will be shown to be practical for titanium, which has a smaller atomic mass.

Choosing the frequency of the rotating electric field and hence the cyclotron frequency as 50 kc., the magnetic flux density will be given by

$$B = \frac{\omega}{\eta}$$

For tantalum $\eta = 5.29 \times 10^5$ coul./kg., therefore,

$$B = \frac{2 \times 3.142 \times 5 \times 10^4}{5.29 \times 10^5}$$

$$= 0.594 \text{ webers/metre}^2.$$

The electron optical column was designed to allow sufficient space for the coils, which will produce such a flux density. The design of the coils will be presented later in this section.

For $r_o = 0.01$ metres, the injection velocity is, from equation (35)

$$v_h = \omega r_o$$

$$= 3.14 \times 10^3 \text{ metres/second}$$

obtainable from a beam voltage, V_h, of 9.33 volts.

From equations (14) and (30), the time taken for the ions to be axially accelerated out of the rotating electric field is given by

$$t_1 = \frac{1}{\sqrt{4\eta A}} \int_0^{0.0125} \left(\frac{L^2 - z^2}{z} \right)^{1/2} dz \qquad (36)$$

where 0.0125 is the height of the rotating-electric-field electrodes in metres. The field strength, E, is determined by equating t_1 to $\frac{r_o B}{E} \cos\phi$ from equation (12). Therefore,

$$\frac{r_o B}{E} \cos\phi = \frac{1}{\sqrt{4\eta A}} \int_0^{0.0125} \left(\frac{L^2 - z^2}{z} \right)^{1/2} dz \qquad (37)$$

For L = 0.065 metres, a = 0.010 metres and V_1 = -20 kv., "A" from equation (15) is 218. Since z is always less than L, the integrand may be expanded and integrated term by term. However, z is small in comparison to L and the first two terms are sufficient. For ϕ small, equation (37) gives

$$E = 8.83 \text{ kv./metre}$$

This is obtainable from a peak voltage of 220 volts on the rotating-electric-field electrodes 2.5 cm. apart.

In Table 1, the design values for titanium are presented with those for tantalum for easy comparison.

TABLE 1

	Tantalum	Titanium
η in coul./kg.	5.29×10^5	2.0×10^6
B in webers/metre^2	0.594	0.594
V_h in volts	9.33	35.3
f_c in kc.	50.0	189
E in kv./metre	8.83	17.1

Returning now to the ray equations and substituting for V, V′, V″, B and η for tantalum, equation (33) becomes

$$r'' + \left[\frac{L^2+z^2}{2z(L^2-z^2)}\right] r' + \left[\frac{3L^2+z^2}{2(L^2-z^2)^2} + 53.5\left(\frac{L^2-z^2}{z}\right)\right] r$$
$$- 9.6 \times 10^{-4}\, I \left(\frac{L^2-z^2}{z}\right)^{3/2} \frac{1}{r} - 53.5\, r_1^4 \left(\frac{L^2-z^2}{z}\right)\frac{1}{r^3} = 0 \qquad (38)$$

and equation (34) becomes

$$r'' - 3.09 \times 10^{-6}\, \frac{I}{r} = 0 \qquad (39)$$

where I in both equations is expressed in microamperes. Equation (38) applies for $0 < z \leqslant 0.055$ m., which is within the magnetic chamber and (39) applies for $z > 0.055$m., which is outside the magnetic chamber in field-free space.

The ray equations are second-order, non-linear, differential equations and, therefore, they were solved numerically on an IBM 1620 (see Appendix 1).

For an ion beam of radius 3.0×10^{-4} m. entering the magnetic chamber $\Delta r = 3.0 \times 10^{-4}$ m. For a pulse width to period ratio of 1.0×10^{-2}, $r_m = 3 \times 10^{-4}$ m., therefore, r_1, at Δz is given by

$$r_1 = r_m + \Delta r$$

$$= 6.0 \times 10^{-4} \text{ m.}$$

Similarly, for a pulse width to period ratio of 2.2×10^{-2} and the same entrance beam radius, $r_1 = 1.0 \times 10^{-3}$m.

The computations were started at $z = \Delta z$ to permit the evaluation of terms containing $\frac{1}{z}$. At $z = 0$, the radius of curvature, r'', becomes infinite because of the assumption made in equation (26). This does not exist physically because the ions are nowhere moving with zero velocity.

The results obtained by solving equations (38) and (39) for the two values of r_1 and for three values of peak current; 1μA., 10μA. and 100μA., are shown in Table 2. The Runge-Kutta method of solution was employed with the initial conditions that at $z = \Delta z$, $r = r_1$ and $r' = 0$.

The condition that $r_1 = 1.0 \times 10^{-3}$ m. and $I = 10\mu A.$ is suitable for use in the system. This case will, therefore, be examined in further detail.

For this case, equation (38) was solved with $\Delta z = 2.5 \times 10^{-3}$m. and the solution indicates that the outer ions in the beam leave the magnetic chamber with a radius of 1.5×10^{-3}m. and a slope of -4.48×10^{-2}. This shows that a waist will be formed outside the chamber. A cross-over

TABLE 2

r_1 in metres	I in μA.	r at z = 0.055m.	r′ at z = 0.055m.	radius r_W of waist in Region III	z at r_W
6.0×10^{-4}	1.0	5.02×10^{-4}m.	-1.83×10^{-2}	4.63×10^{-8}m.	0.0827m.
"	10.0	1.70×10^{-3}m.	-4.52×10^{-2}	7.15×10^{-8}m.	0.0932m.
"	100.0	7.99×10^{-3}m.	-1.99×10^{-1}	4.11×10^{-7}m.	0.0954m.
1.0×10^{-3}	1.0	6.51×10^{-4}m.	-2.67×10^{-2}	1.21×10^{-7}m.	0.0794m.
"	10.0	1.50×10^{-3}m.	-4.48×10^{-2}	3.22×10^{-7}m.	0.0890m.
"	100.0	6.76×10^{-3}m.	-1.69×10^{-1}	5.70×10^{-7}m.	0.0953m.

point is not possible because from equation (39), it can be seen that the radius of curvature becomes infinite as r tends to zero.

Equation (39) was solved with $\Delta z = 2.5 \times 10^{-3}$m. in the region 5.5×10^{-2}m. $\leqslant z \leqslant 8.5 \times 10^{-2}$m., $\Delta z = 2.5 \times 10^{-4}$m. in the region 8.5×10^{-2}m. $\leqslant z \leqslant 8.9 \times 10^{-2}$m. and $\Delta z = 1.0 \times 10^{-5}$m. for 8.875×10^{-2}m. $\leqslant z \leqslant 9.2 \times 10^{-2}$m. The solution indicates a waist of radius 3.22×10^{-7}m. formed at $z = 8.9 \times 10^{-2}$m. This is 3.4 cm. outside the magnetic chamber. The ion lens of focal length 7.5 cm. will focus this waist on the substrate.

In section 3.3.3, it was stated that equation (9) and (10) held for ions injected into the system at $r_o \pm \Delta r$, if the origin of the rectangular coordinate system was shifted by $\pm \Delta r$. Therefore, $\dot{\theta}$ is with reference to the shifted axis rather than the axis being used. It will now be shown that the angular velocity plays a small part in the trajectory of the ions.

From equation (21), $\dot{\theta}$ for the outer ions at the exit of the magnetic chamber is given by

$$\dot{\theta} = \frac{\eta B}{2} \left(1 + \frac{0.001^2}{0.0015^2} \right)$$

and the velocity, v_θ, at the same point is

$$\dot{\theta} r = 1.08 \times 10^{-3} \eta B$$

When the ions enter Region III, this velocity will cause the beam to diverge with a slope given by

$$\frac{\dot{\theta} r}{\sqrt{2\eta |V|}} = 1.16 \times 10^{-3}$$

which represents 2.59% of the slope with which the beam is convergent.

A peak current of 10μA. with a pulse width to period ratio of 0.022 has an average value of 0.22μA. This current will deposit tantalum at the rate of 15.2Å/min. over 0.1 cm.^{2} area of substrate.

The design of the coils producing the magnetic field will now be presented.

For the dimensions shown in Figure 7, the reluctance of the magnetic circuit is given by

$$R = \frac{0.108}{0.008^2 \pi \mu_o} + \frac{1}{0.00635 \pi \mu_1} \int_{0.00794}^{0.073} \frac{dr}{r}$$

$$+ \frac{0.108}{\pi \mu_1 (0.0762^2 - 0.07145^2}$$

where the first term on the right is the reluctance of the air gap, the second term is the reluctance of the top and bottom of the chamber and the last term is the reluctance of the chamber wall. All the numbers are expressed in metres, μ_o is the permeability of free space and μ_1 is the permeability of the magnetic material from which the chamber is built. Therefore,

$$R = \frac{1690}{\pi\mu_o} + \frac{352}{\pi\mu_1} + \frac{154}{\pi\mu_1}$$

$$= \frac{1690}{\pi\mu_o} + \frac{506}{\pi\mu_1}$$

For Armco iron, $\frac{\mu_1}{\mu_o}$ will vary from 1200 - 4000 along the magnetic return path, therefore, the reluctance of the return path is negligible in comparison to that of the air path.

The magnetomotive force is given by

$$\text{mmf.} = \frac{BL}{\mu_o}$$

where L = 0.108 m. and $\mu_o = 1.257 \times 10^{-6}$ henry/metre. Therefore,

$$\text{mmf.} = \frac{0.594 \times 0.108}{1.257 \times 10^{-6}}$$

$$= 51,030 \text{ ampere-turns}$$

Assuming that about 20% of this value is lost in flux leakage, then 61,200 ampere-turns will have to be provided.

Using $\frac{1}{8}$" outer diameter copper tubing with wall thickness 0.032" and 0.0016" enamel insulation, each coil will accommodate 262 turns. The current required will be 116.8 amperes.

The resistance of each coil will be 0.186 ohms and the power dissipated per coil will be 2.54 kw. For cooling, tap water will be circulated through and around the copper tubing at 0.2 gal./min. This is for a temperature rise in the water of 40°C. Detailed calculations for the design of coils are presented in Appendix 2.

3.4 An Alternate Bending Mechanism

For a charged particle in a uniform magnetic field,

$$\omega_c = \eta B = \frac{v_\theta}{r} = \frac{k}{r}$$

where v_θ is the velocity in the θ direction and is equal to a constant k, since the charged particle cannot gain energy from a static magnetic field. Therefore,

$$r = \frac{k}{\eta B} \qquad (40)$$

Let us consider an ion moving along a line of constant magnetic field strength on an axially symmetrical magnetic hump, which increases towards the axis of symmetry. If the ion is perturbed so that r decreases, the ion encounters a stronger magnetic field and r further decreases. It follows that under the proper conditions, an ion may gyrate around a magnetic hump with decreasing radius.

The last paragraph is a rather simple extension of equation (40) and is not strictly correct. If the ion gains any radial velocity, then v_θ is no longer constant and (40) does not remain valid.

In the $r - \theta$ plane, the only force acting on the ion is the Lorentz force, therefore,

$$F_r = - q\, v_\theta B_z = M(\ddot{r} - r\dot{\theta}^2) \qquad (41)$$

from which

$$\ddot{r} = r\dot{\theta}^2 - \eta\, r\dot{\theta} B_z \qquad (42)$$

From Busch's theorem,

$$\dot{\theta} = \frac{\eta}{r^2} \int_{r_o}^{r} B_z \, r dr + \frac{r_o^2}{r^2} \dot{\theta}_o \tag{43}$$

where r_o and $\dot{\theta}_o$ are the radius and angular velocity at $t = 0$. Equation (42) may, therefore, be written in the form

$$\ddot{r} = f(r) \tag{44}$$

since both B_z and $\dot{\theta}$ are functions of r.

The simplest form of the solution of equation (44) gives t as a function of r. That solution may be obtained in the following manner:

Let $\frac{dr}{dt} = y$

Then $\frac{dy}{dt} = f(r)$

$$\frac{dy}{dt} \cdot \frac{dt}{dr} = \frac{f(r)}{y}$$

therefore, $y . dy = f(r) \, dr$

or $\frac{y^2}{2} = \int f(r) \, dr$

i.e. $\left(\frac{dr}{dt}\right)^2 = 2 \int_{r_o}^{r} f(r) \, dr + \dot{r}_o^2$

therefore,

$$t = \int_{r_o}^{r} \frac{dr}{\sqrt{2 \int_{r_o}^{r} f(r) \, dr + \dot{r}_o^2}} \tag{45}$$

In the present problem $\dot{r}_o = 0$, therefore, equation (45) reduces to

$$t = \int_{r_o}^{r} \frac{dr}{\sqrt{2 \int_{r_o}^{r} f(r)\, dr}} \tag{46}$$

Equation (46) indicates a return of the ion as in the case of the rotating electric field system, hence, the ion must be accelerated axially into field free space when the radius is about zero.

To obtain $f(r)$, the functional dependence of B_z upon r must be specified. Assuming

$$B_z = B_o\, e^{-br^2} \tag{47}$$

and substituting in (43)

$$\dot{\theta} = \frac{\eta B_o}{r^2} \int_{r_o}^{r} e^{-br^2}\, r dr + \frac{r_o^2}{r^2}\, \dot{\theta}_o$$

$$= - \frac{\eta B_o}{2b} \frac{e^{-br^2}}{r^2} + \frac{1}{r^2} \left(r_o^2\, \dot{\theta}_o + \frac{\eta B_o}{2b}\, e^{-br_o^2} \right) \tag{48}$$

Let
$$A = r_o^2\, \dot{\theta}_o + \frac{\eta B_o}{2b}\, e^{-br_o^2} \tag{49}$$

then
$$\dot{\theta} = - \frac{\eta B_o\, e^{-br^2}}{2b\, r^2} + \frac{A}{r^2} \tag{50}$$

and $$\dot{\theta}^2 = \frac{\eta^2 B_o^2}{4b^2} \frac{e^{-2br^2}}{r^4} + \frac{A^2}{r^4} - \frac{\eta A B_o}{b} \frac{e^{-br^2}}{r^4} \tag{51}$$

Substituting (50) and (51) into (42) gives

$$\ddot{r} = \frac{\eta^2 B_o^2}{4b^2} \frac{e^{-2br^2}}{r^3} + \frac{A^2}{r^3} - \frac{\eta A B_o}{b} \frac{e^{-br^2}}{r^3} + \frac{\eta^2 B_o^2 e^{-2br^2}}{2br}$$

$$- A \eta B_o \frac{e^{-br^2}}{r} \tag{52}$$

therefore,

$$f(r) = \frac{\eta^2 B_o^2}{2b} \left(\frac{e^{-2br^2}}{2br^3} + \frac{e^{-2br^2}}{r} \right) - \eta B_o A \left(\frac{e^{-br^2}}{br^3} + \frac{e^{-br2}}{r} \right) + \frac{A^2}{r^3} \tag{53}$$

$$2 \int_{r_o}^{r} f(r) dr = - \frac{\eta^2 B_o^2}{4b^2} \left(\frac{e^{-2br^2}}{r^2} - \frac{e^{-2br_o^2}}{r_o^2} \right) + \frac{\eta B_o A}{b} \left(\frac{e^{-br^2}}{r^2} - \frac{e^{-br_o^2}}{r_o^2} \right)$$

$$- A^2 \left(\frac{1}{r^2} - \frac{1}{r_o^2} \right) \tag{54}$$

Substituting (54) into (46)

$$t = \int_{r_o}^{r} \frac{dr}{\left[B\left(\frac{e^{-2br^2}}{r^2} - \frac{e^{-2br_o^2}}{r_o^2} \right) + C \left(\frac{e^{-br^2}}{r^2} - \frac{e^{-br_o^2}}{r_o^2} \right) + D\left(\frac{1}{r^2} - \frac{1}{r_o^2} \right) \right]^{1/2}} \tag{55}$$

$$\text{Where} \quad B = -\frac{\eta^2 B_o^2}{4b^2}$$

$$C = \frac{\eta B_o A}{b}$$

$$D = -A^2$$

The magnetic field as described resembles a "plasma bottle" (a longitudinal field with magnetic mirrors at both ends), which is almost always associated with trapped particles. However, the ion is not trapped within the "bottle", but achieves a minimum radius, which then grows until the ion is out of the magnetic field. For the trapping of an externally originating particle within a "plasma bottle", something violent must happen to the particle or the magnetic field, neither of which occurs in the present case.

The digital computer study of equation (55) shows that the ion does go to a minimum radius. However, the energy of the ion in the $r - \theta$ plane remains constant, unlike the case of the rotating electric field system. At the exit of the system, the trajectory of the ion is, therefore, inclined to the z-axis. Because of this and the anticipated difficulty in achieving a magnetic hump of the correct shape, this approach was abandoned.

CHAPTER 4

THE MAIN ELECTRON BEAM AND MICROMACHINING

The main electron beam will be used for electron-beam micromachining, and as the electron probe for the scanning electron microscope and the microanalyser. Among the three modes of operation, the requirements for the machining mode are the most difficult to realize. Consequently, once the requirements for the machining mode are fulfilled, operation in the other modes will be easily achieved.

4.1 Requirements for Electron-Beam Micromachining

The accuracy to which narrow strips of the thin film may be generated through electron-beam micromachining is a very important consideration in the design and manufacture of thin-film integrated circuits. For a given size component, the accuracy of machining sets a low limit on the accuracy of the component value and hence a low limit on power requirements. For a given accuracy in component value, the accuracy of machining sets a low limit on component size.

For accurate electron-beam machining, it is necessary to pulse the beam, so that the spot on the

substrate where the beam impinges is brought to a very high temperature, which lasts for only a short time. This allows evaporation of the material without maintaining a molten pool, the size of which will limit machining accuracy.

For the micromachining of thin-film elements, power densities of the order of 10^9 watts/cm^2 must be achieved in a sharply defined spot a few hundred Angstroms in diameter. At high voltages (about 150 kv.), this requirement is easily achieved, but the range of the electrons at such voltages is quite long in most materials to be machined. As a result, a large portion of the beam energy will be dissipated below the surface and cause the material there to be explosively expelled, which will again lead to poor machining accuracy.

In a multilayered thin-film structure, it may be necessary to strip away material from one layer without affecting the underlying layers. For such an application, a low voltage beam must be used. W.C. Nixon et al. (20) have succeeded in using a 5 kv. beam to machine aluminium films to a depth of 400 - 600 Å.

Table 3 gives the approximate range of electrons with varying energies in aluminium and tantalum. The values for aluminium were obtained from A. Berthelot (21) and those for tantalum were calculated on the assumption that the range expressed in mass per unit area is the same for both materials.

TABLE 3

Energy of the electron in kev.	Range in mg/cm²	Range in Aluminium	Range in Tantalum
10	0.17	0.63μ	0.10μ
20	0.6	2.2μ	0.36μ
40	2.3	8.5μ	1.4μ
60	6.0	22μ	3.6μ
80	10	37μ	6.0μ
100	13	48μ	7.8μ
120	51	190μ	31μ
140	110	410μ	67μ
160	200	740μ	121μ

The theory developed to date in electron-beam machining is inadequate to quantitatively explain the experimental results obtained. K.H. Steigerwald (8) has plotted the energy balance of the different processes which occur during electron-beam heating of steel. Some of the data were experimentally obtained while others were calculated. L.G. Pittaway (22) has done some theoretical studies of the temperature distribution in thin foils bombarded by an electron beam. Here again rather specific assumptions were made.

4.2 The Electron Optical Column

Figure 9 shows a diagram of the electron optical column. The lower portion extending below the baseplate is a modified version of the column from the Mikros EM-20 electron microscope. The column is 4" square and carries a cylindrical lens tube, which houses the anode of the electron gun, a variable aperture diaphragm and the first electrostatic condenser lens. The gun assembly which carries the filament and the Wehnelt electrode for the gun forms a vacuum seal at the lower end of the column.

The upper column extending within the belljar is a 6" diameter tube, which, as far as the main beam is concerned, houses the final electrostatic condenser lens, the deflection plates and the stage with the substrate carrier. In addition, the upper column encloses the magnetic chamber and other parts of the ion optical system, parts of the electron-probe micro-analyser and the electron-collection system for the scanning electron microscope.

4.3 The Lens Assembly

The lens column contains two Einzel unipotential electron lenses, the outside electrodes of which are at ground potential. The centre electrode of the first lens is connected to the negative high voltage supply (cathode potential) and the centre electrode of the second lens is connected to the negative

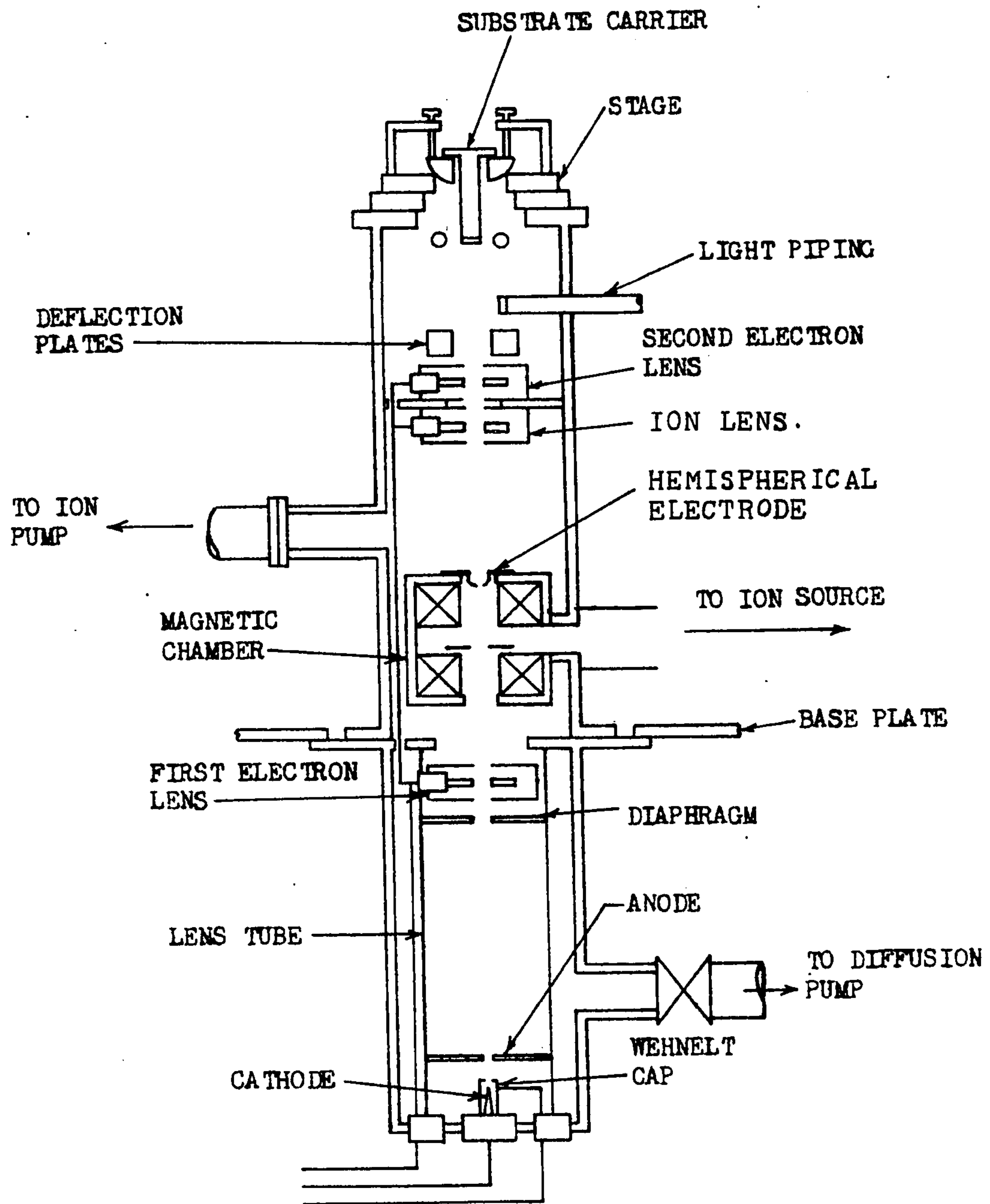

FIGURE 9

The electron optical column

high voltage supply through a voltage divider for varying the power of the second lens and hence the working distance (the distance between the final lens and the substrate).

The first lens is a strong one; focal length 0.6 cm. and coefficient of spherical aberration 4.5 cm. It is positioned 30 cm. from the cathode. The second lens has a focal length of 5.57 cm. and a coefficient of spherical aberration 20.3 cm. It is positioned 45 cm. from the first lens.

With a working distance of 5 cm., the total demagnification obtainable with these two lenses is 357. If the working distance is reduced to 3 cm., the demagnification increases to 500.

4.4 The Electron Gun

The Langmuir relation (23) for the maximum obtainable current density in a demagnified image of a cathode is

$$I = I_o \left(\frac{\epsilon V}{kT} + 1 \right) \sin^2 \alpha \qquad (56)$$

where I is the maximum current density obtainable in the spot, I_o is the emission current density at the cathode, V is the beam voltage at the spot, k is Boltzmann's constant, T is the Absolute temperature of the cathode and α is the half angle subtended by the cone of electrons which converge on the focused spot.

For $\epsilon V \gg kT$ and small angles, equation (56) reduces to

$$I = I_o \frac{\epsilon V}{kT} \alpha^2 \quad (57)$$

The hairpin filament, made from 0.005" tantalum wire may be operated at 2800^oK, at which temperature, the saturation emission current density is 16 amps/cm.^{2}. At a working distance of 3 cm., the mechanical aperture of the final lens is 0.023 radians. Therefore, at 60 kv., the maximum obtainable current density is

$$I = \frac{16 \times 6 \times 10^4 \times 2.3^2 \times 10^{-4}}{8.6 \times 10^{-5} \times 2800}$$

$$= 2120 \text{ amps/cm.}^2 \quad (58)$$

which gives a power density of 1.27×10^8 watts/cm.^{2}.

The electron gun and lens assembly were designed to operate at 40 kv. but may be operated at voltages up to 60 kv. However, at this voltage, the range of the electron is quite long as shown in Table 2. The use of a field emission cathode will reduce T and increase I_o in equation (57) leading to a much higher current density at the focused spot. This will allow the use of lower beam voltages for machining. Experiments using a field emission cathode will be performed at a later date.

The filament is welded to a hermetic seal centered in the Wehnelt cap, which fits into the gun assembly. The gun assembly is mechanically aligned to the bottom end of the lens tube. Adjustment screws are provided for centering

the anode, which is located in the lens tube.

Proposed modifications to the electron gun are discussed in section 4.9.

4.5 The Deflection System

For post deflection, the lateral deflection of the beam, d, is given by

$$d = \left(\frac{LD}{2} + \frac{L^2}{4} \right) \frac{E_p}{V_k} \tag{59}$$

where L is the length of the deflection plates, D is the distance from the substrate to the nearest point of the deflection plates, E_p is the electric field strength between the deflection plates and V_k is the potential of the electron beam (cathode potential).

In the lens column, D is 0.02 metres, and L is 0.015 metres. Therefore, equation (59) reduces to

$$d = 2.06 \times 10^{-4} \frac{V_p}{sV_k} \tag{60}$$

where V_p is the voltage applied to the deflection plates and s is the distance between opposite plates. For V_p = 670 volts (section 5.1), Figure 10 shows the variation of the lateral deflection, d, with plate spacing, s, for different values of beam potential V_k.

For deflections of less than 0.5 mm. the aberrations caused by the deflection system is negligible since the angle of deflection from the axis is less than 1.5 degrees.

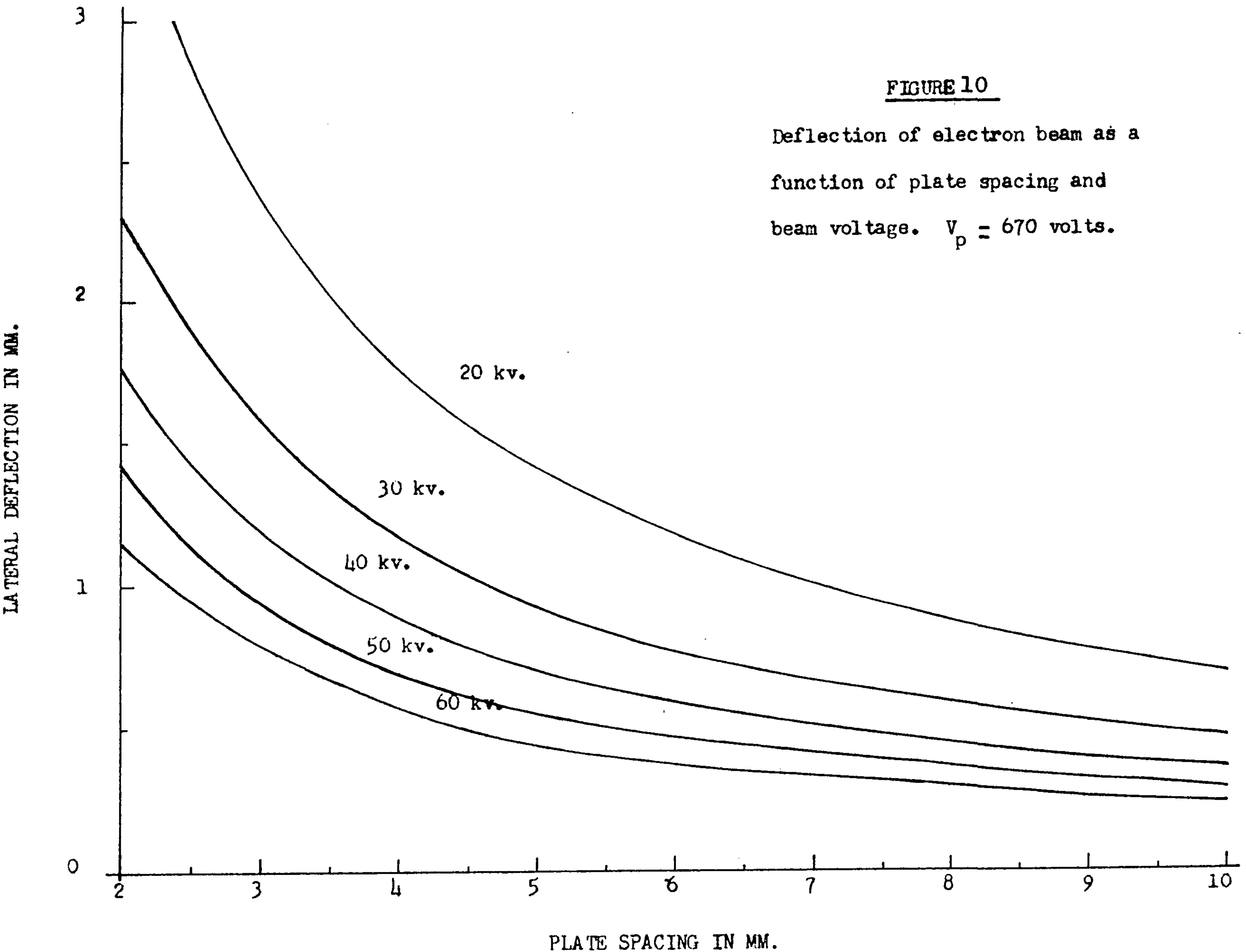

FIGURE 10

Deflection of electron beam as a function of plate spacing and beam voltage. $V_p = 670$ volts.

Figure 11 is a photograph of the second-electron-lens carrier, the second electron lens and the deflection electrodes assembly. Figure 12 shows the unit disassembled. The carrier, 1, with its levelling screws, 2, rests on a platform in the upper electron optical column. The locking screws, 3, attach the lens carrier to this platform. The electron lens, 4, fits snugly into the carrier and the boron nitride structure, 5, in turn, forms a tight fit over the electron lens. The boron nitride cap, 6, locks the eight brass deflection electrodes in position.

The use of eight electrodes will allow versatility in pattern generation. For scanning, four electrodes may be removed or adjacent electrodes may be electrically connected to form four electrodes, which gives a better electrical field configuration than the four individual electrodes.

4.6 The Substrate Carrier and Stage

Figure 13 is a photograph of the substrate carrier and stage mounted in position at the top of the electron optical column. Figure 14 is a photograph of the unit disassembled and Figure 15 is an illustration.

The base of the stage, 3, is aligned with the axis of the electron optical column and forms a vacuum seal with the flange at the top of the column. On the base, sits the carriage, 4, for x-axis translation which is achieved by a micrometer drive, 11, against a spring loaded plunger similar

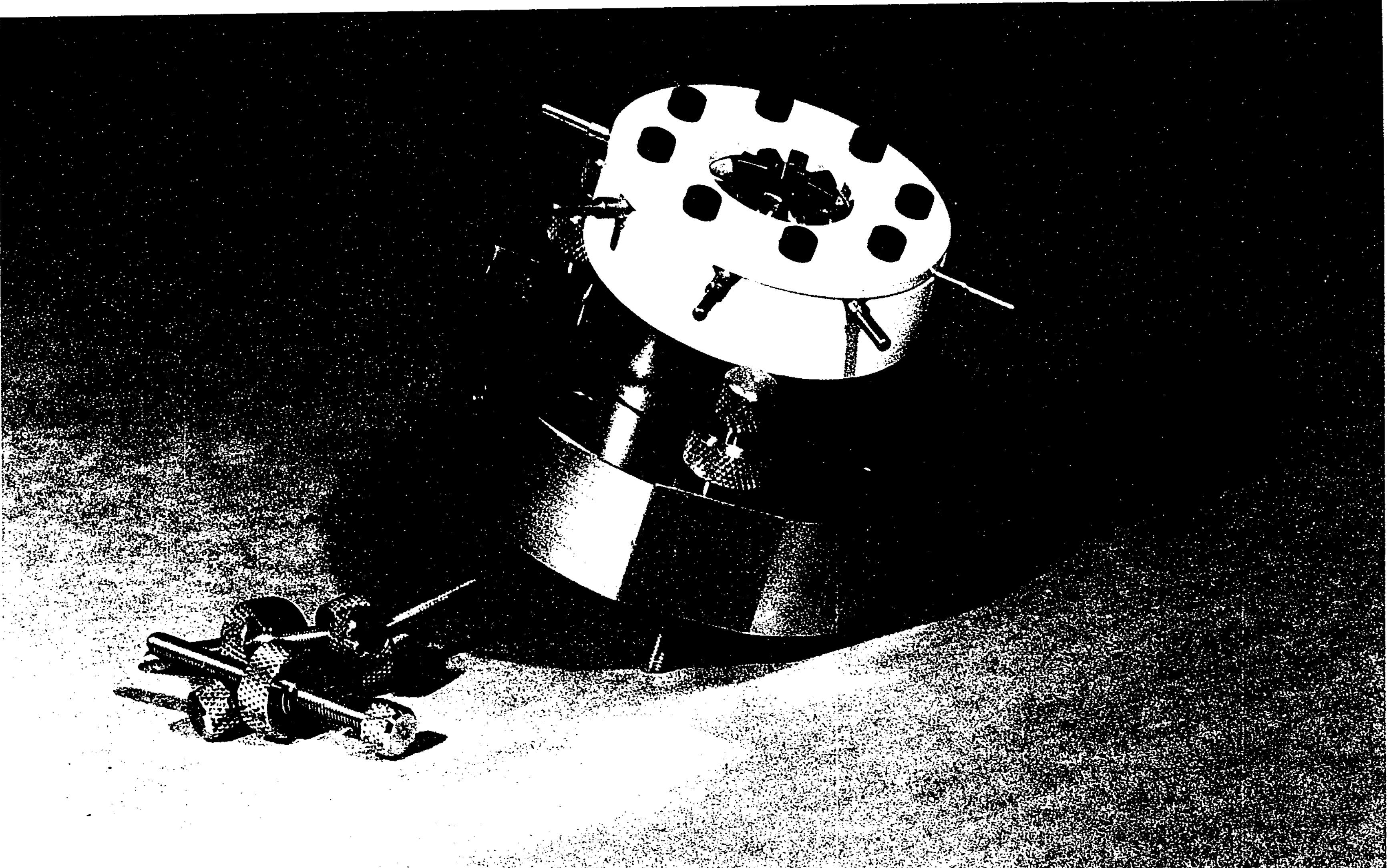

FIGURE 11

The second electron lens and deflection electrodes assembly

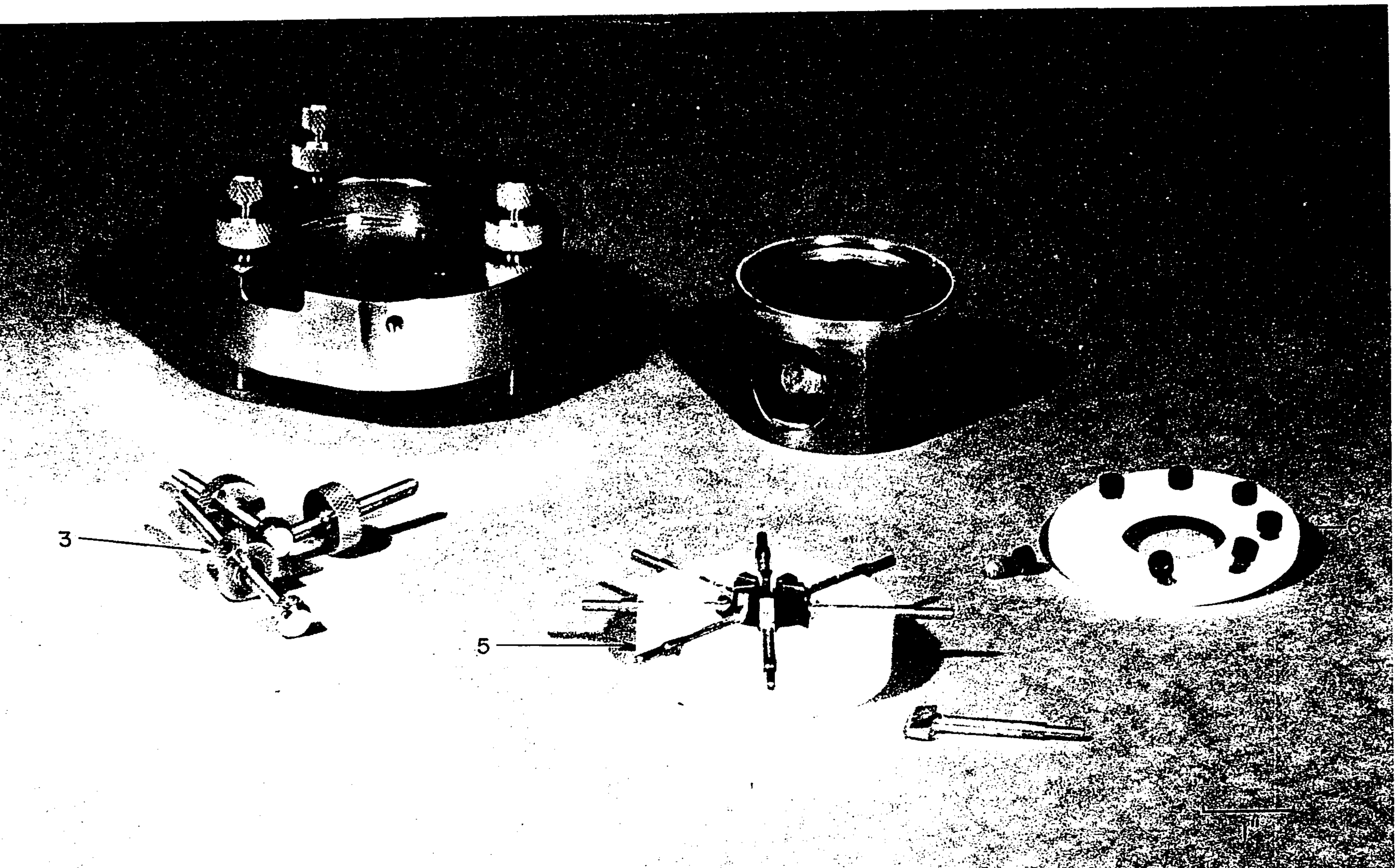

FIGURE 12

The second electron lens and deflection electrode system disassembled

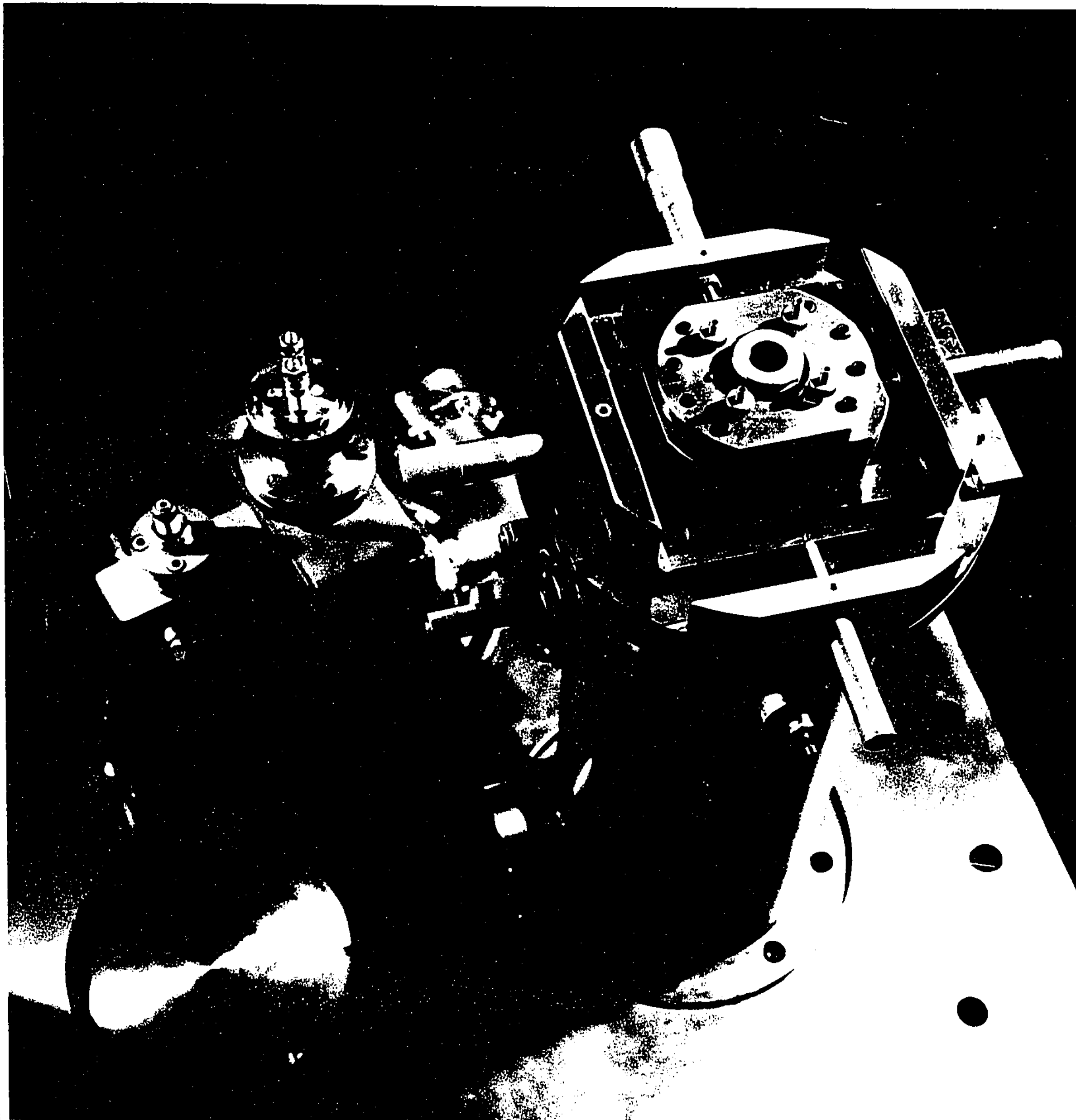

FIGURE 13

The substrate carrier and stage assembly
in position

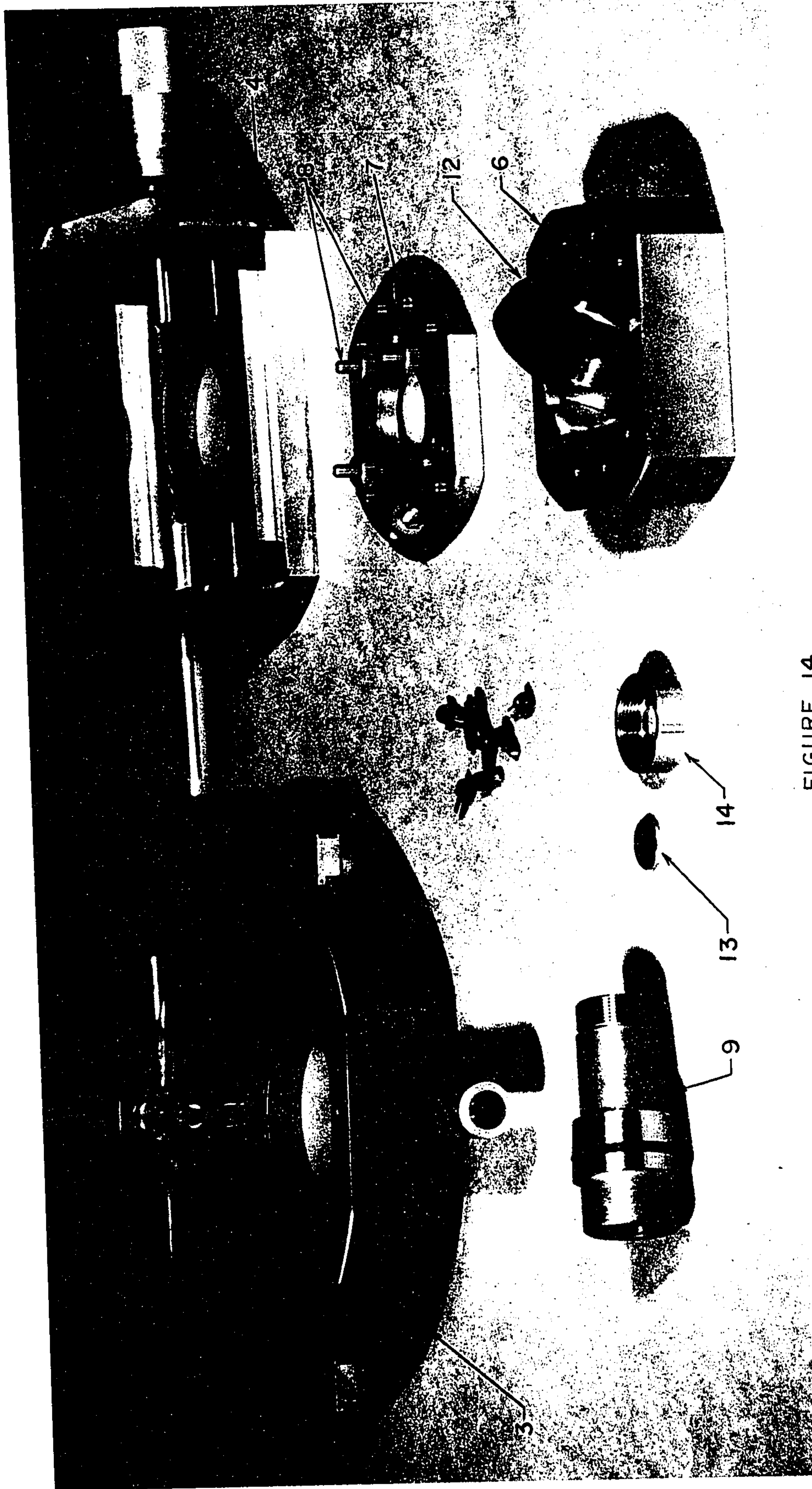

FIGURE 14
The substrate carrier and stage disassembled

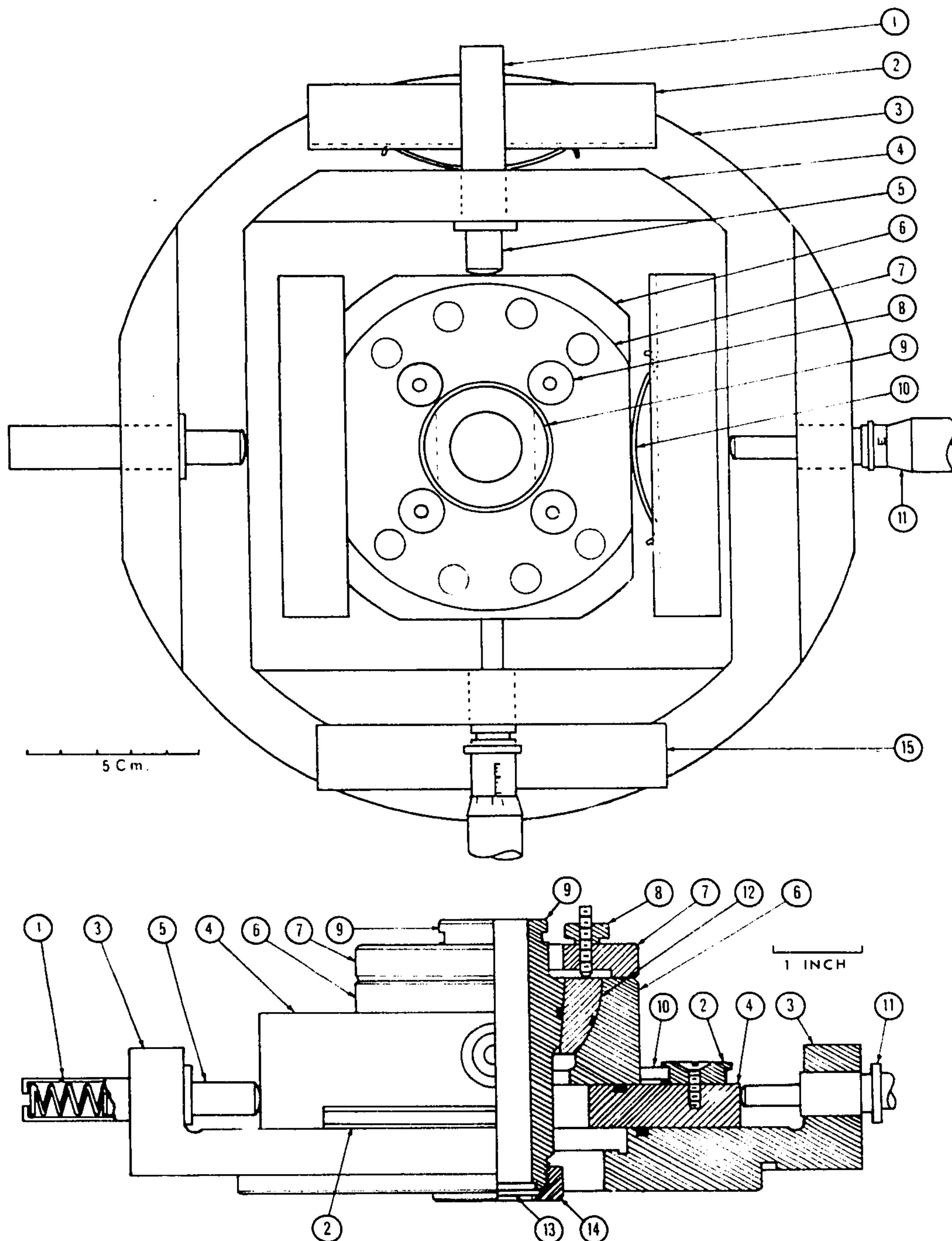

FIGURE 15

The substrate carrier and stage

1. Spring-loaded plunger holder, 2. Restraining-spring runner,
3. Base of the stage, 4. Carriage for x-axis translation,
5. Spring-loaded plunger, 6. Carriage for y-axis translation,
7. Retaining plate for tilt-adjust system, 8. Tilt-adjust screws,
9. Substrate carrier, 10. Restraining spring, 11. Micrometer drive, 12. Hemispherical holder for substrate carrier,
13. Substrate, 14. Substrate retainer, 15. Constraining rail.

to 5. During translation, the carriage is constrained by a spring similar to 10 and the rail, 15.

The carriage for y-axis translation, 6, rests on the carriage for x-axis translation and is driven by a micrometer screw similar to 11, against the spring loaded plunger, 5. This carriage is constrained by the spring, 10, and a rail similar to 15.

The hemispherical holder, 12, for the substrate carrier, 9, fits into the y-axis carriage and provides tilt adjustments by means of the screws, 8. The substrate is held in place by the retainer, 15.

The stage provides $\pm$ 1.0 cm. translation in the x- and y- directions and 5° tilt adjustments for the substrate. With maximum tilt, translation is reduced to $\pm$ 0.5 cm.

When the MMP is operated without the belljar, as for example, during the alignment of the components in the electron optical column, "O" rings are inserted in the grooves in the various components of the stage.

4.7 Power Supplies

The power supplies for the main electron beam are shown schematically in Figure 16.

T_1 is a specially built transformer with 60 kv. insulation between the primary and secondary windings. It is capable of supplying up to 100 watts for heating the hairpin filament. This transformer is fed from a variac,

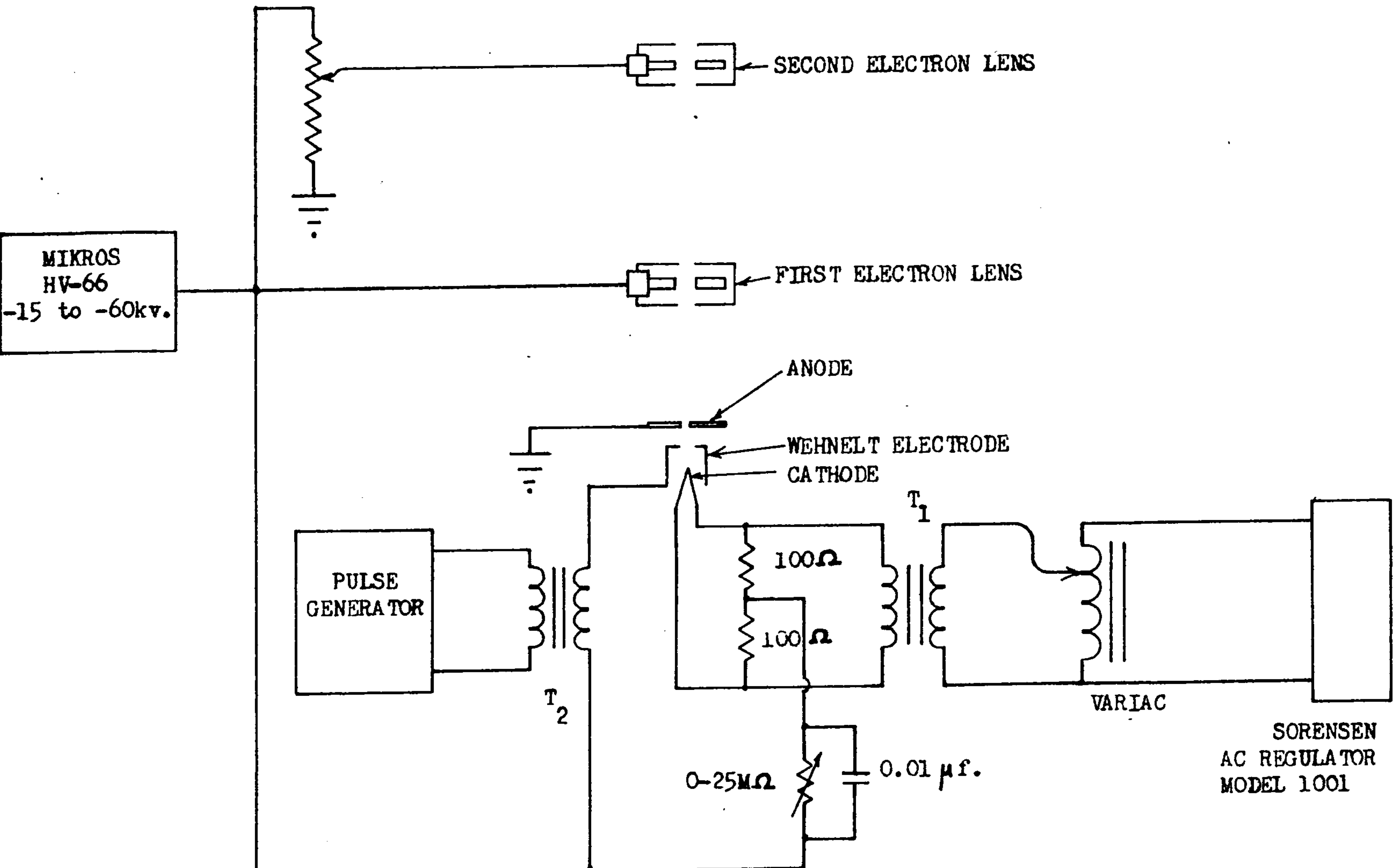

FIGURE 16

Power supplies for the main electron beam

which in turn is fed from a Sorensen A.C. Regulator, model 1001.

The negative high-voltage supply is the Mikros HV-66 model, which gives 1 mA. at 15 - 60 kv. with a 0.05% load regulation from no load to half load and 0.01% line regulation for a 10% line variation. The negative high voltage is connected to the cathode through a bias resistor (CTS high voltage variable resistor, 0 - 25 MΩ) and two balanced 100 Ω resistors. The balanced resistors maintain the tip of the filament at the same potential as the point between the resistors, and, therefore, avoid distortion of the field between the anode and the filament.

The negative high voltage is connected to the Wehnelt electrode through the secondary windings of the pulse transformer, T_2, which also has 60 kv. insulation between the primary and secondary windings. The pulse transformer together with a pulse generator is used for pulsing the electron beam at rates varying from 1 kc. to 20 kc. The pulse generator and the pulse monitor are discussed in section 5.3.

4.8 Alignment of the Beam

Figure 17 shows the test-target carrier, which is provided for beam alignment. The test-target carrier is mounted in the base of the stage, which also carries a microscope for viewing spot formation. The test-target carrier may be used with a transparent glass target, a

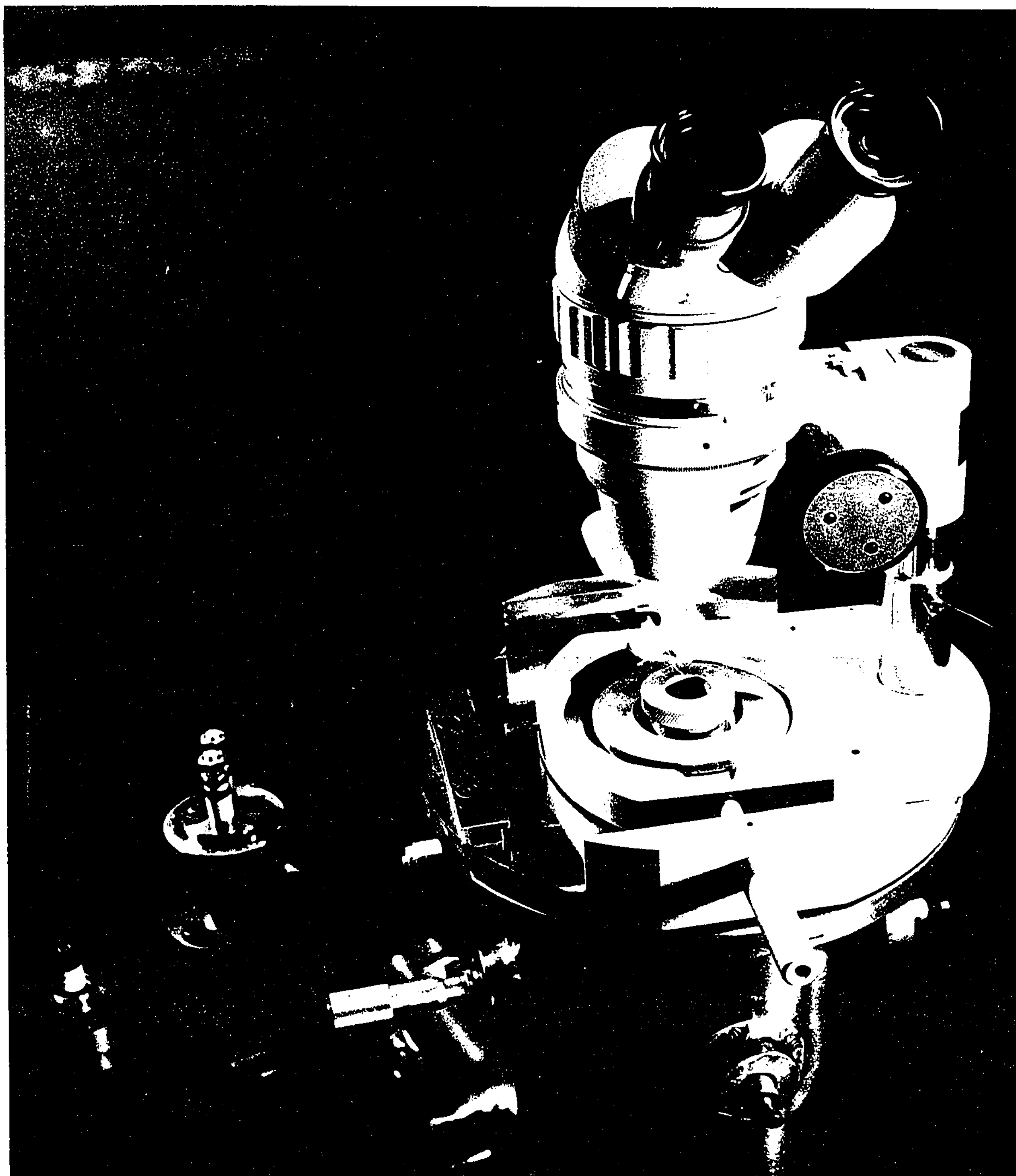

FIGURE 17

The test target carrier and microscope

phosphorescent target or a Faraday cup.

For beam alignment, a transparent glass target is placed in the test-target carrier and with the filament of the electron gun glowing, the anode, the electron lenses and the diaphragm are aligned so that the filament is clearly seen in the centre of all the apertures. This aligns the mechanical axis of the instrument and forms a good starting point for the alignment of the electron optical axis. The transparent glass target is then replaced with one coated with a phosphor (zinc sulphide was found satisfactory) and the beam is turned on. Fine adjustments are then made until a circular spot is seen on the phosphor. The final step is the adjustment of the focal length of the second electron lens for minimum spot size.

4.9 Performance of the Machining Beam

The beam was aligned as described in section 4.8 and a Faraday cup was placed in the test-target carrier. The beam current measured 0.05μA. in a spot size about one micron. The beam voltage at this time was 20 kv., therefore, the power density in the spot was about 1.27×10^5 watts/cm.^{2}.

This power density was sufficient for the scanning electron microscope, the results of which are given in section 5.4. However, the power density must be increased by three or four orders of magnitude for the machining mode of the beam.

In the electron gun, the distance between the Wehnelt electrode and the cathode is fixed and at this distance, the

optimum bias is zero. The Wehnelt electrode is being redesigned to allow a variable distance so that a negative bias may be applied to the Wehnelt electrode. This will reduce the spot size and hence increase the power density at the spot.

Voltages higher than 20 kv. could not be used due to some defects in the Mikros HV-66 power supply. These defects will be corrected so that higher voltages may be used, again leading to a higher power density.

CHAPTER 5

THE SCANNING ELECTRON MICROSCOPE AND MICROANALYSER

A brief description of the scanning electron microscope was given in section 1.3.1. In this chapter, the scanning electron microscope in the MMP will be discussed in detail.

Figure 18 is a block diagram of the display system and Figure 19 is a photograph of the display rack. The electron beam of the C.R.T. scans a television-like raster in synchronism with the main beam scanning a selected portion of the specimen. Either secondary or reflected (back-scattered) electron may be collected and used to intensity modulate the C.R.T.

When the main beam is used as the electron probe in the scanning electron microscope, the beam voltage is reduced below 20 kv. to avoid radiation and thermal damage to the specimen surface. The pulse generator is turned off and the beam is continuous rather than pulsed. Apart from these two factors, the operation of the beam is exactly as described in Chapter 4.

The Analab model 1220 is a storage oscilloscope with a grey scale and intensity-integrating capabilities.

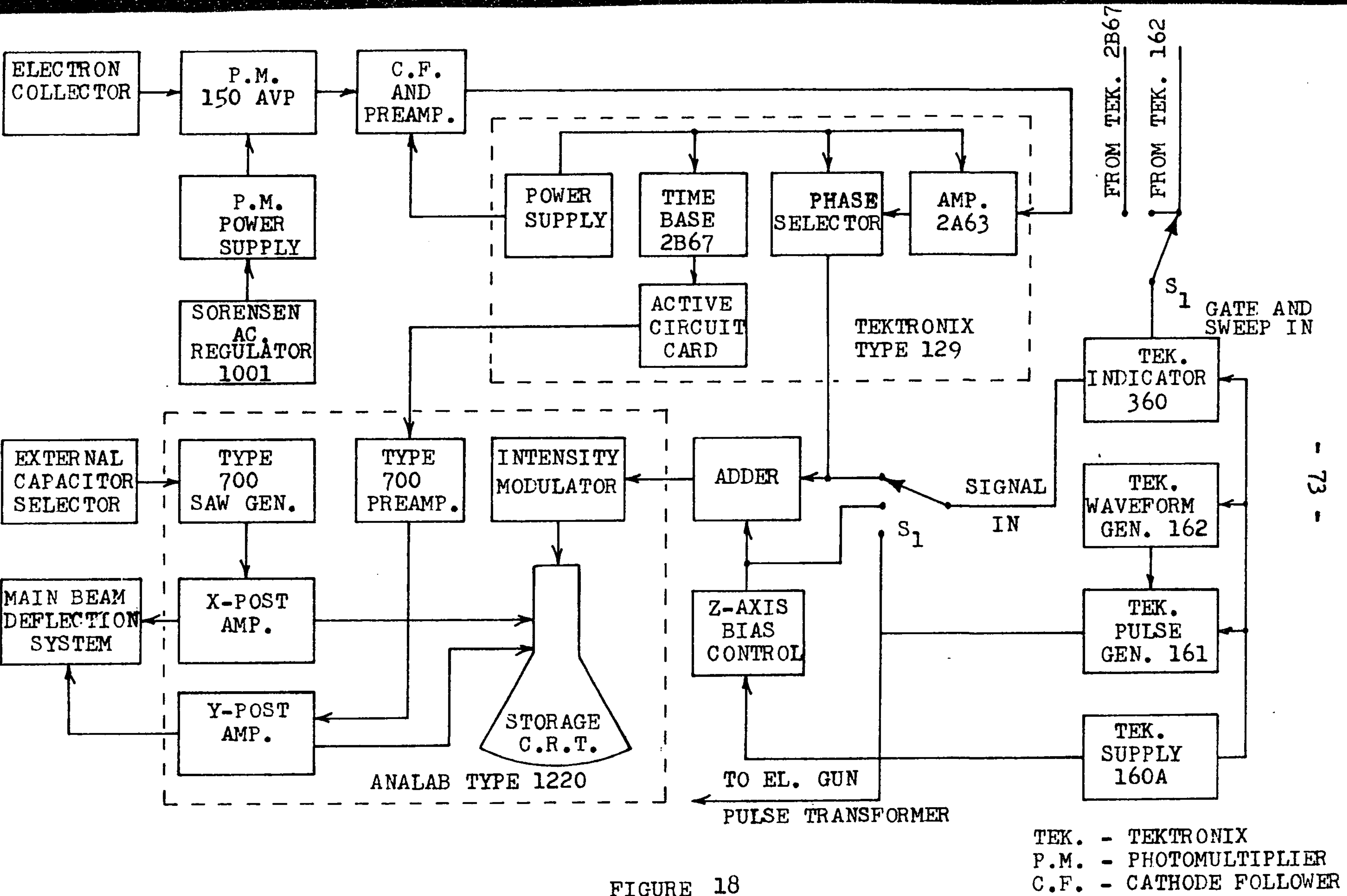

FIGURE 18

System diagram of the display assembly

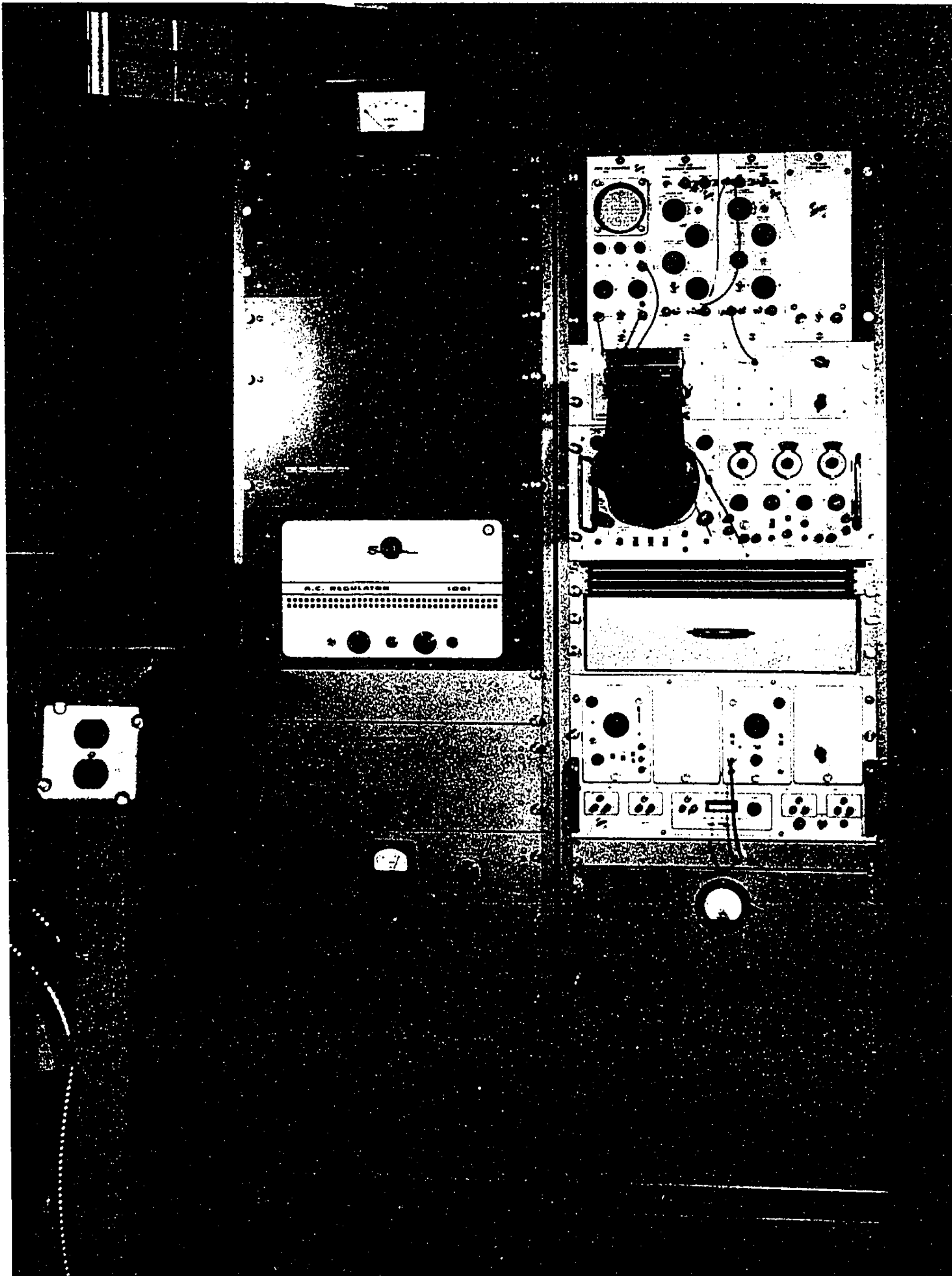

FIGURE 19

The display assembly

Because of these properties, this C.R.O. is used to gradually build up an image of the specimen when the signal to noise ratio of the modulating signal is low. A small signal to noise ratio is expected when the collected current is comparable to the dark current of the photomultiplier.

Recording speeds varying from one frame in 7.5 minutes to one frame in 2.5 seconds are possible on the Analab oscilloscope. The lower speed is limited by the slowest available sawtooth waveform for controlling the frame rate. The upper speed, however, is limited by the oscilloscope itself.

The C.R.T. in the Analab oscilloscope is pulsed so that the beam current during the duty period is sufficient for recording yet the average power dissipated at the screen is low enough to avoid permanent damage to the screen. The information stored on the Analab oscilloscope is, therefore, in a sampled form.

With the minimum spot size and at writing speeds below one cm. per millisecond, the samples merge into each other and a single trace on the C.R.T. appears continuous. The beam is pulsed at a fixed rate of 16 kc. and for no "dark lines", a scan rate of 25 lines per cm. or greater is required. A single frame, 6 cm. x 10 cm., traced out in 2.5 seconds, therefore, contains 40,000 samples. Any faster frame rate results in dark spaces.

On the Analab oscilloscope, the maximum magnification obtainable will be 8,000 when the main beam spot size of

500 Å. is finally achieved.

For viewing the specimen at frame rates comparable to television reception, a C.R.T. with a continuous beam will be coupled as a slave to the C.R.T. in the Analab oscilloscope.

5.1 The Scanning System

The x and y post amplifiers in the Analab oscilloscope are identical and for a full scale (10 cm.) deflection, the output from the amplifiers is 670 volts. The deflection system for the main beam is driven directly from these amplifiers. Therefore, there is a one to one correspondence between the position of the main beam on the specimen and the position of the beam on the C.R.T. either during a scanning period or when the beams are stationary.

The x-axis drive originates in the sawtooth generator of the Analab 700 plug-in unit. This sawtooth is amplified by the x-post amplifier and then used to control the frame rate. The slowest rate available from the plug-in is one frame in 50 seconds. However, with external capacitors, the rate may be decreased to one frame in 7.5 minutes.

The y-axis sawtooth originates in a type 2B67 Tektronix time base generator powered by a type 129 Tektronix plug-in unit power supply. This sawtooth is amplified by the Analab type 700 plug-in preamplifier and the Analab y-axis post amplifier and then used to control the scan rate. The sawtooth available from the 2B67 varies from one scan in

50 seconds to one scan in 10μ seconds.

The combined system is capable of scanning at rates varying from one frame in 7.5 minutes to 400 frames per second.

5.2 The Electron Collector

The use of secondary electrons for intensity modulating the C.R.O. gives finer details than reflected electrons (24). This is because with a small positive potential on the collector, almost all of the secondary electrons may be collected regardless of the direction in which they were emitted. On the other hand, reflected electrons travel in almost straight paths with their trajectories little affected by the potential on the collector. Only those electrons initially travelling towards the collector, reach the collector. Therefore, the information carried by all the other electrons is lost.

In the MMP, reflected electrons are used for routine inspection and control of pattern generation. When finer details are required, the system will be modified to collect secondary electrons.

The electron collector was designed after the system described by T.E. Everhardt and R.F.M. Thornley (25). T.E. Everhardt et al. (24) have shown that an electron collector consisting of a scintillator connected to a photomultiplier by light pipe gives better performance than the

direct application of an electron multiplier. One of the main reasons for this is the small solid angle subtended by the first dynode of the electron multiplier at the target point on the specimen. In the case of the scintillator-photomultiplier combination, the scintillator may be placed quite close to the specimen to subtend a considerably larger solid angle.

The collector system in the MMP uses a block of NE 102 scintillation material mounted close to the specimen and connected to the photomultiplier by polyvinyltoluene light pipe. The scintillation block is cemented to the polyvinyltoluene rod with Carl Biggs' resin No. R-823* which has a high bonding strength and a refractive index of 1.56. The refractive index of NE 102 is 1.58.

5.2.1 The Photomultiplier, Cathode Follower and Preamplifier Assembly

A cathode follower is used to isolate the photomultiplier circuit from the preamplifier, the three circuits being housed in the same shielded case. Figure 20 is the circuit diagram of the photomultiplier, cathode follower and preamplifier assembly.

* The use of R-823 for bonding the scintillator to the light pipe was suggested by Mr. M.J.C. Ewer of Nuclear Enterprises, Winnipeg, Canada, the manufacturer of both NE 102 scintillation material and polyvinyltoluene light pipes.

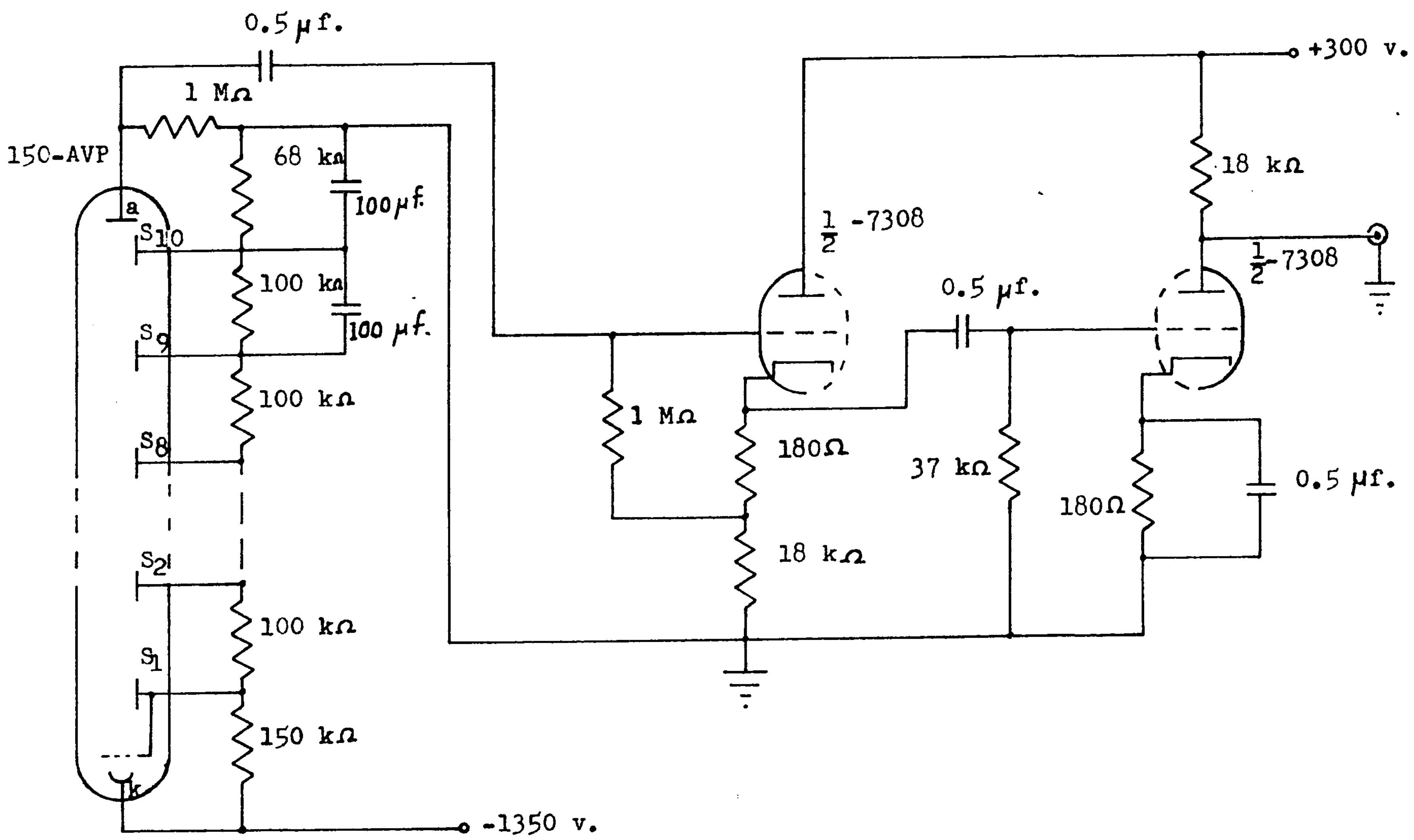

FIGURE 20

The photomultiplier, cathode follower and preamplifier assembly

The photomultiplier tube is a Philips 150-AVP, which has its maximum sensitivity at the same wavelength, 4300 Å, as that for the maximum emissivity of NE 102 scintillation material. The tube has 10 stages and is operated at 120 volts per stage except the first stage, which is operated at 180 volts. The photomultiplier tube is shielded with a mu-metal case.

The cathode follower has a gain of 0.93 and an output impedance of 600 ohms. The gain of the preamplifier is 20.

5.2.2 The Z-Axis Amplifier

The z-axis amplifier is a Tektronix type 2A63 plug-in unit powered by the type 129 power supply.

5.3 Intensity Modulation of the C.R.O.

Either a positive or a negative image of the specimen may be obtained on the C.R.T. by choosing a signal with the proper phase. The phase selector has two outputs; one for intensity modulating the Analab oscilloscope and the other for the slave C.R.T. Either C.R.T. may be modulated with a positive or a negative image independently of the other.

A dc. voltage is provided so that the C.R.T. may be biased in the centre of the linear portion of the grey

scale.

A type 360 Tektronix indicator is used for monitoring the modulating signal and the bias voltage. The type 360 indicator is powered by a Tektronix type 160A power supply and the sawtooth and gate to the indicator are supplied from the type 2B67 time base plug-in unit which drives the y-axis of the Analab oscilloscope.

The type 360 indicator is also used for monitoring the pulse duration of the main beam during machining. During this mode of operation, the sawtooth and gate to the indicator are supplied by a Tektronix type 162 waveform generator, which also supplies the trigger to a Tektronix type 161 pulse generator. The output from the type 161 is applied through the isolating pulse transformer to the Wehnelt electrode of the main electron gun for pulsing the beam.

5.4 Performance of the Scanning Electron Microscope

Figure 21 shows an image of the zinc sulphide phosphor used to align the electron optical axis. The picture was taken at 100 magnification with the specimen in the test-target carrier.

A copper grid on which specimens are mounted for a transmission electron microscope was then placed in the substrate carrier and a picture was taken at 100 magnification. This is shown in Figure 22. Figure 23 shows the same specimen at 200 magnification

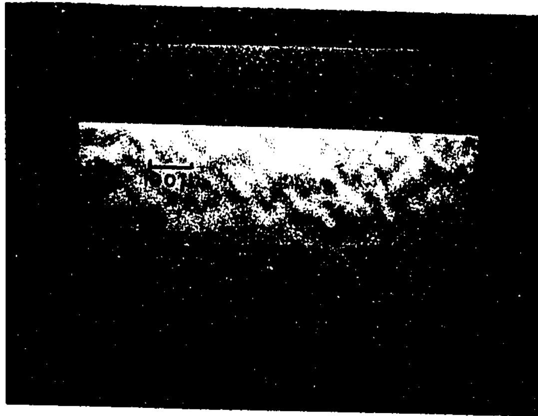

FIGURE 21

The zinc sulphide phosphor used to align the scanning electron microscope

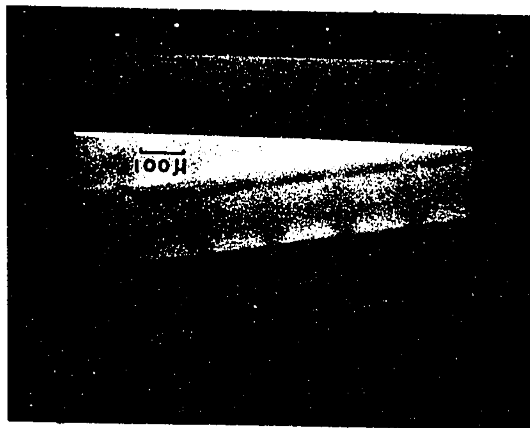

FIGURE 22

Copper grid taken at one hundred magnification

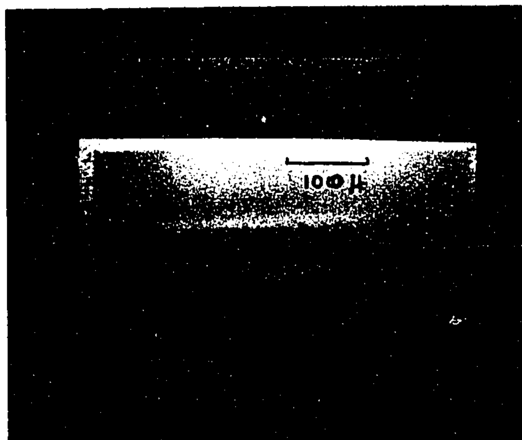

FIGURE 23

Copper grid taken at two hundred magnification

The resolution of the instrument as estimated on the display scope is about one micron corresponding to the size of the electron probe. It is expected that this resolution will be improved by the new design of the Wehnelt electrode as explained in section 4.9.

5.5 Provision for the Microanalyser

For determining the purity of films and for inspection of multilayered thin-film structures, the main beam will be used as the electron probe for the microanalyser. The original design of the MMP specified the installation of crystal detectors for x-ray analysis. However, another electron collector matched to the one currently in use in the scanning electron microscope will be installed for microanalysis (see section 1.3.2).

CHAPTER 6

THE VACUUM SYSTEM

The degree of vacuum in which thin films are prepared is one of the important factors in determining the properties of the films. P.A. Redhead et al. (26) have calculated that at a pressure of one torr, it takes 1.3 microseconds for a clean surface to be covered with a monomolecular layer of air (calculations made for nitrogen) assuming that every molecule which arrives at the surface sticks to it. At 1×10^{-6} torr, it takes 1.3 seconds and at 1×10^{-11} torr, it takes 36 hours. These figures give an indication of the ease with which the residual gas in a vacuum system may affect the composition of thin films during deposition.

Reactive sputtering makes use of this gettering action during the deposition of films. However, even when a gas is introduced into the system for varying film properties, the composition of the residual atmosphere must be carefully controlled. J.G. Needham (27) has reported good reproducibility in a sputtering chamber which is evacuated to 1×10^{-9} torr.

In the MMP, the region around the substrate will be evacuated to a pressure of 1×10^{-9} torr in an effort to

maintain the surface of the deposited films clean. Surrounding this region is a vacuum of 2×10^{-7} torr.

6.1 The High-Vacuum Assembly

Figure 24 shows the component parts of the vacuum system. Both the belljar and the baseplate are made from stainless steel. The belljar is 24 inches in diameter and 24 inches high and has strip heaters with a total capacity of 7.5 kilowatts strapped to the outside surface. The belljar has two 7 inch ports: one is for visual observation and the other connects to a vacuum lock, through which raw material will be transported into the system.

The seal between the belljar and the baseplate is a single water-cooled butyl rubber "O" ring. It has been estimated that water-cooled butyl rubber has a lower outgassing rate than Viton A. To minimize vibration of the system, the baseplate is mounted to the frame through vibration insulators.

6.1.1 Vacuum Pumps

A 4 inch diffusion pump (NRC model HS4-750) rated at 750 litres per second is used to evacuate the high-vacuum region. This pump is operated with Dow Corning DC-704 fluid and is fitted with a water-cooled cold cap and a molecular sorbent baffle (sodium zeolite trap) both for minimizing the

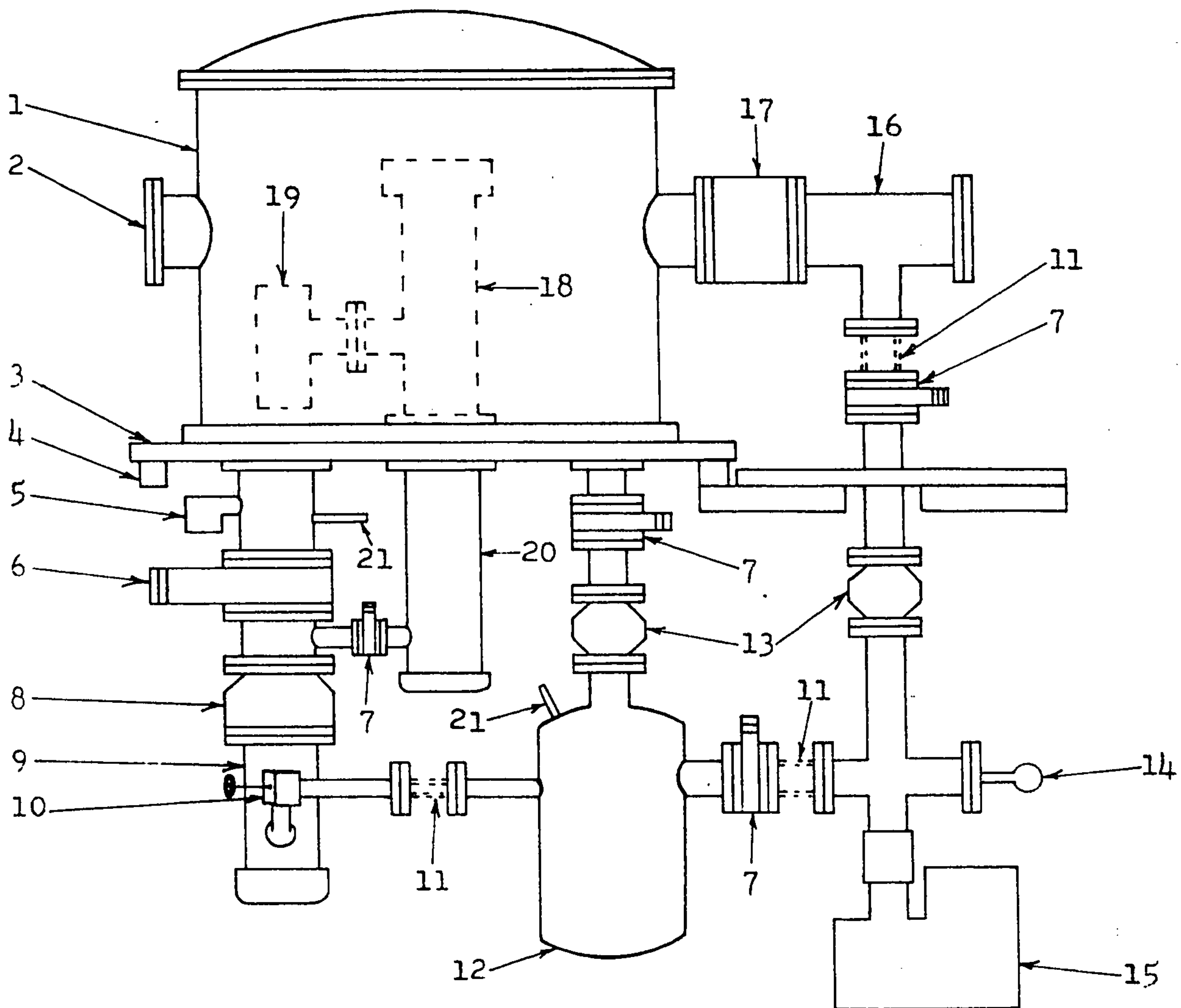

FIGURE 24

Component parts of the vacuum system

1. Belljar, 2. Siteport, 3. Baseplate, 4. Vibration mount, 5. Spectrometer tube, 6. 4" Gate valve, 7. 2" Gate valve, 8. Molecular sorbent baffle, 9. Diffusion pump, 10. Rt. angle valve, 11. Bellows, 12. Ballast tank, 13. Cold baffle, 14. Discharge tube, 15. Mechanical pump, 16. Vacuum lock, 17. 6" Gate valve, 18. Upper lens column, 19. Ultrahigh vacuum ion pump, 20. Lower lens column, 21. Thermocouple gauge.

backstreaming of pump fluid.

The diffusion pump exhausts into a 60 litre ballast tank, which is pumped by a mechanical pump (Welch model 1398M) rated at 1400 litres per minute. The ballast tank was designed so that during operations requiring a high resolution, the mechanical pump may be turned off. When the mechanical pump is off, the system should be able to operate for a calculated period of 180 hours before the pressure in the ballast tank rises from 1×10^{-3} torr, the "blank off" pressure in the ballast tank, to 0.45 torr, the maximum forepressure for the diffusion pump. Actually, 4 hours of operation was achieved with no detectable change in the pressure in the ballast tank. This is sufficient for most processes in the MMP.

6.1.2 Vacuum Gauges

The system is equipped with an NRC type 710B gauge control, which operates two type 501 thermocouple gauges and one type 507 ionization gauge. Thermocouple gauge No. 1 reads the foreline pressure in the ballast tank and thermocouple gauge No. 2 reads the pressure on the high-vacuum side of the diffusion pump. The thermocouple gauges are used to indicate when it is safe to turn on the diffusion pump and the ionization gauge.

The thermocouple gauges have a range from one torr to 1×10^{-3} torr and the ionization gauge is usable between

5×10^{-3} torr and 1×10^{-7} torr in five ranges.

An Alphatron type 530 gauge also measures the foreline pressure in the ballast tank. This gauge uses a small charge of radium 226 as a source of alpha particles for ionization. Therefore, the use of the Alphatron gauge is not limited to low pressures as in the case of ionization gauges with heated cathodes. The Alphatron gauge measures pressures from 1×10^{3} torrs to 1×10^{-4} torr in seven ranges and, therefore, covers a region of the pressure scale not covered by the other gauges.

6.2 The Ultrahigh Vacuum

The upper lens column is made from nickel-plated mild steel and is pumped by a Boostivac High Vacuum Ion Pump model 10-401. This is an "evapor-ion" pump, which enhances the action of an ion pump by providing the added gettering action of a freshly deposited metal film. In the Boostivac pump, the rate of evaporation of a titanium film is variable whereby pumping speeds ranging from 40 litres per second to 145 litres per second are available.

An ion pump is essentially an ionization gauge and, therefore, does not require any additional gauging. The current in the cold cathode discharge of the Boostivac pump is used to indicate the pressure in the ultrahigh vacuum region. The pump measures pressures from 1×10^{-4} torr to 1×10^{-9} torr.

6.3 Residual-Gas Analysis

In the analysis of film characteristics, it is important to know the composition of the atmosphere in which the film was prepared. For the analysis of the residual gas in the vacuum system, an Aero Vac Vacuum Analyzer model AVA 1 is used. The instrument is a mass spectrometer which also has facility for measuring total pressures. The use of this instrument for leak detection is discussed under section 6.4.

Two mass ranges, 2 to 11 and 12 to 70, are available on the Vacuum Analyzer by manually interchanging deflecting magnets. The sensitivity of the instrument for partial pressure measurement is 10^{-10} torr for nitrogen.

6.4 Leak Detection

Compensating a leaky vacuum system with large capacity pumps does achieve the required degree of vacuum, but, it does not permit any control of the atmosphere in the vacuum system. It is, therefore, necessary to locate and repair leaks in the system. For leak detection, the Vacuum Analyzer is used with helium as the probe gas. The instrument is tuned to the partial pressure of nitrogen and the system is probed with the helium gas. A decrease in the partial pressure of nitrogen indicates a leak. The sensitivity of the instrument in this mode of operation is 1×10^{-9} torr as compared to 1×10^{-8} torr if the instrument is tuned to

the partial pressure of helium and the increase in partial pressure is observed.

The spectrometer tube of the Vacuum Analyzer may be connected to the high-vacuum side of the diffusion pump or to the ultrahigh-vacuum region in the lens column.

For large leaks which maintain the foreline pressure at a sufficiently high value to support a glow discharge, a Tesla coil in conjunction with a glow discharge tube is mounted to the neck of the mechanical pump and the system is probed with acetone. If the probe vapour enters the system through a leak, the reddish purple colour of the discharge, which is characteristic of air, takes on a whitish appearance due to the presence of the acetone.

A Rustrak strip chart recorder (amplifier model 98 and recorder model 88) is used to measure the rates of slow leaks in the system. The recorder monitors the pressure as indicated by either the Alphatron gauge or the type 507 ionization gauge. This recorder also forms part of the protective circuitry discussed in the next section.

6.5 Protective Circuitry

If for any reason, the pressure on the high-vacuum side of the diffusion pump exceeds 1.5×10^{-4} torr, the power to the main electron gun and to the diffusion pump is turned off. Under the high-pressure condition, the pump fluid breaks down and the filament of the electron gun may burn out.

Figure 25 shows the protective circuit for the electron gun and the diffusion pump.

A-A is the normal operating position of the switch S_3. The position B-B is provided for starting and other conditions which require bypassing protection from pressure rise in the system. 115 v.ac. is supplied to the contacts A-A of the switch S_3 whenever power is being supplied to the filament of the ionization gauge. If power is being supplied to S_3, and S_4 is closed, the normally opened switch S_2 closes and supplies power to the electron gun and the diffusion pump.

If the pressure in the high vacuum region rises above 1.5×10^{-4} torr, the power to the filament of the ionization gauge is turned off and so is the voltage to the contacts A-A. The switch S_2 opens and the electron gun and the diffusion pump are turned off.

The normally closed switch S_4 is a thermal relay which protects the system if the water to the cooling coils of the diffusion pump and the cold cap is turned off. S_4 is installed in the exhaust line of the cooling system together with a heater coil. If the water is turned off, the temperature rises and at a preset temperature, S_4 opens and turns off the system.

During bake-out of the vacuum system, a thermocouple is imbedded near the butyl rubber "O" ring between the belljar and the baseplate. The temperature is monitored on a Rustrak temperature recorder model 147.

Both the temperature recorder and the pressure

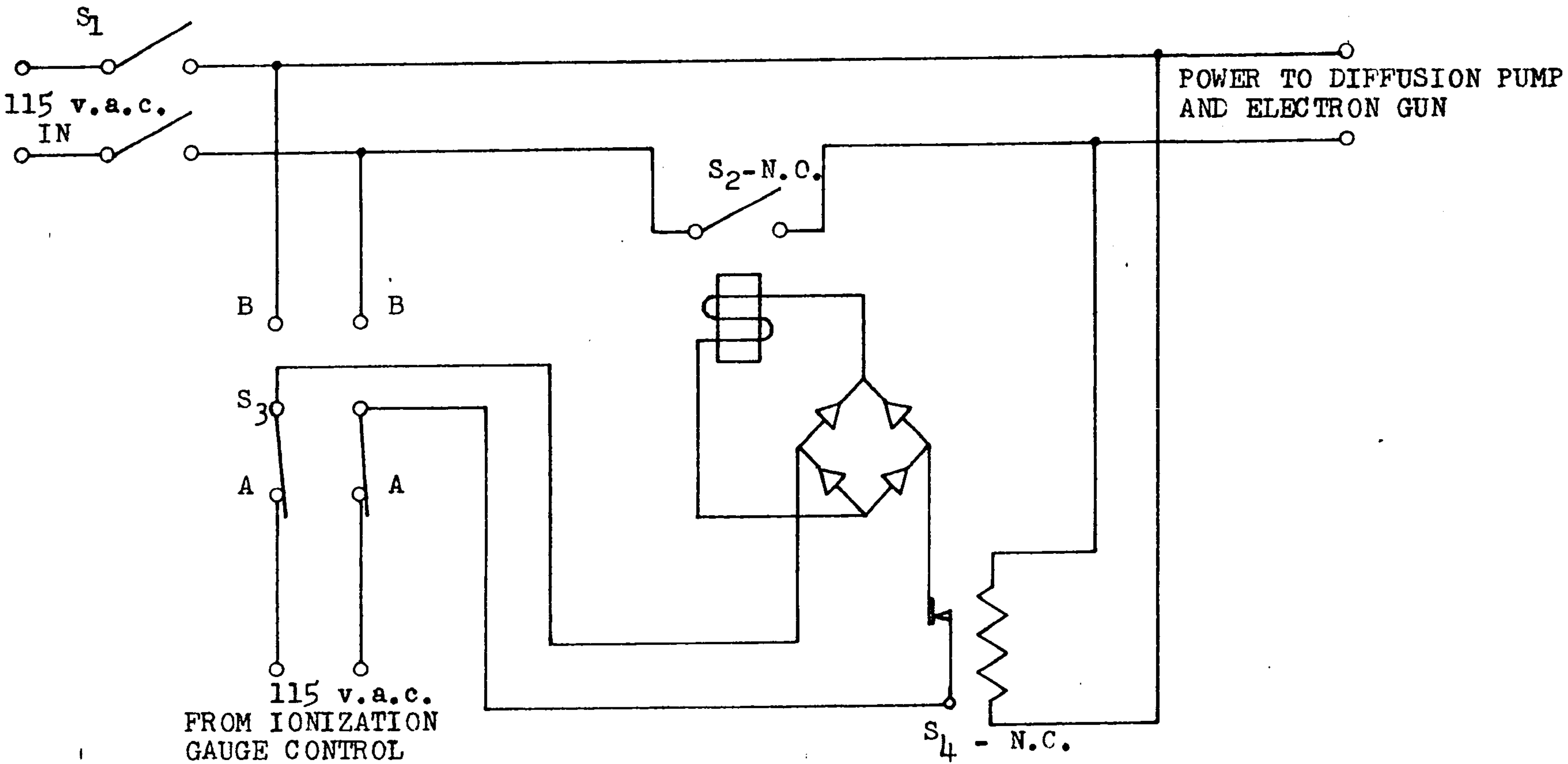

FIGURE 25

Protective circuit for the diffusion pump and electron gun

recorder are equipped with relays for controlling the functions between preset limits. The temperature recorder is set so that the heaters are turned off if the temperature rises above 100°C and are turned on again when the temperature drops below 100°C. The pressure recorder is set so that the heaters are turned off if the pressure exceeds 1×10^{-4} torr and are turned on again when the pressure drops below this value. The bake-out operation is automatically terminated when the pressure drops below 5×10^{-7} torr in the belljar. The protective circuitry operative during bake-out is shown in Figure 26.

During regeneration of the sodium zeolite in the molecular sorbent baffle, the protective circuitry used during bake-out is also used. A thermocouple is imbedded between the baffle heaters and the baffle and the temperature is controlled below 350°C. The regeneration process is automatically terminated when the pressure in the foreline of the diffusion pump drops below 5×10^{-3} torr.

Figure 27 shows the control and monitor racks for the vacuum system.

6.6 Performance of the Vacuum System

After the vacuum system has been briefly exposed to the laboratory atmosphere, the mechanical pump takes the system down to 5×10^{-2} torr in two minutes. The diffusion pump is turned on at that pressure and it takes half an hour

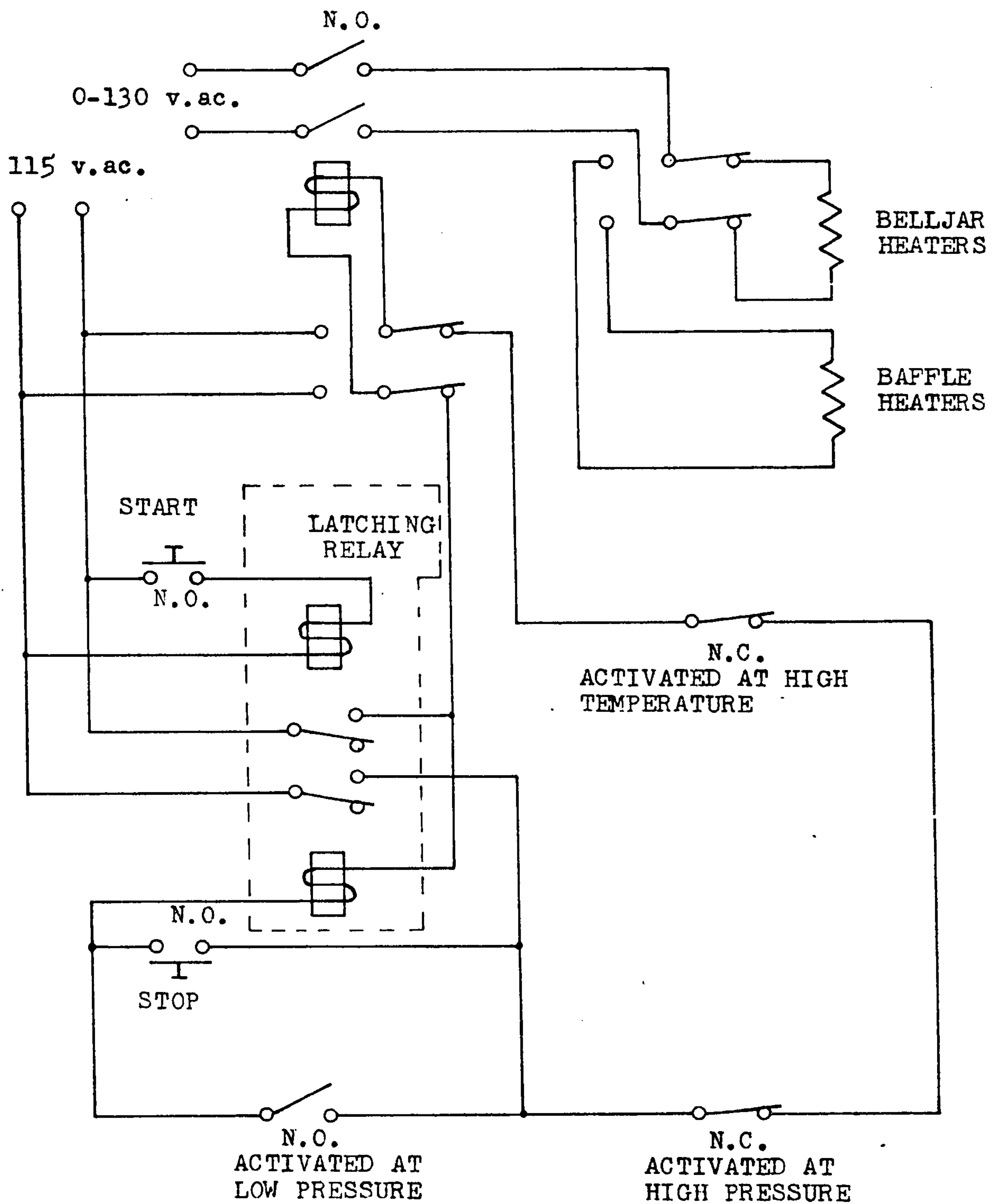

FIGURE 26

Protective circuitry operative during bake-out of the belljar and during regeneration of the sodium zeolite in the molecular sorbent baffle

FIGURE 27

Control and monitor racks for the vacuum system

to pump the system down to 3×10^{-6} torr. The blank-off pressure of the high-vacuum system after the belljar and the molecular sorbent baffle have been baked out, is 2×10^{-7} torr.

When the vacuum is broken with dry nitrogen, as is done if access to the chamber is not required, the pump-down time is reduced to 10 minutes from atmospheric pressure to 1×10^{-6} torr and 3 minutes from 1×10^{-3} to 1×10^{-6} torr.

The system was designed so that the four inch diffusion pump may be replaced by a six inch pump for faster pump-down times without the necessity of remachining the baseplate.

Figures 28 and 29 show the analysis of the residual gas in the high vacuum chamber when the total pressure in the system was 1×10^{-6} torr.

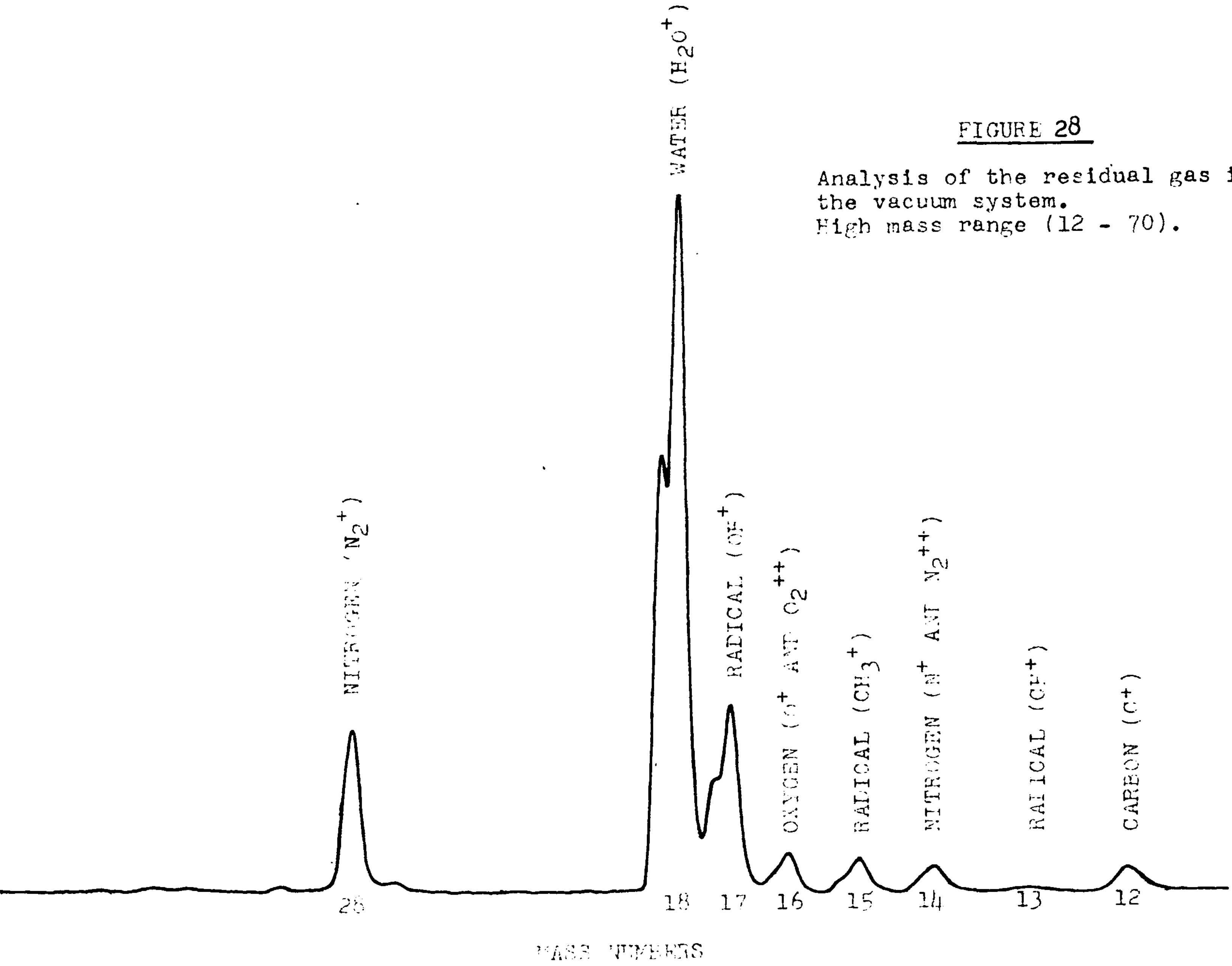

FIGURE 28

Analysis of the residual gas in the vacuum system.
High mass range (12 - 70).

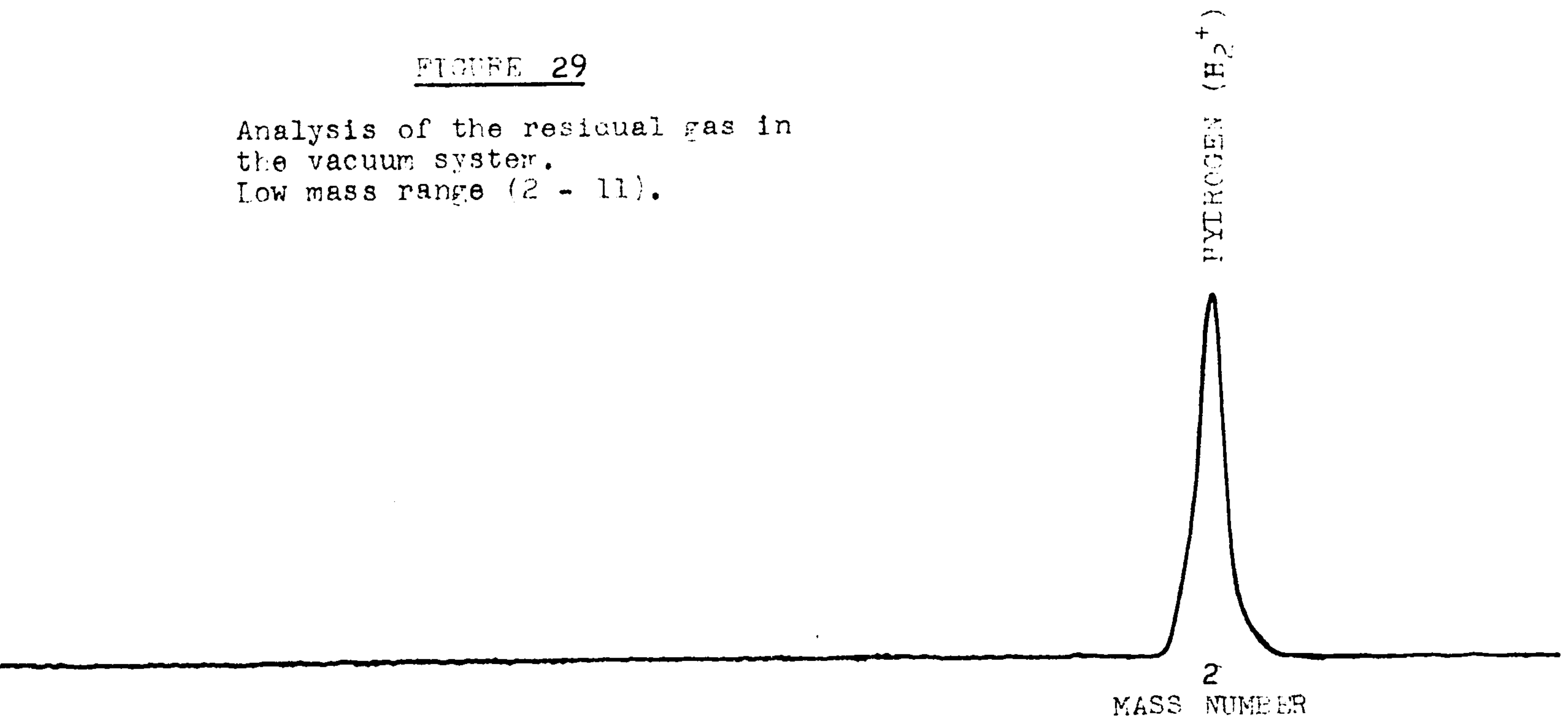

FIGURE 29

Analysis of the residual gas in the vacuum system.
Low mass range (2 - 11).

CHAPTER 7

DISCUSSION

The basic ideas for the MMP were originated early in 1962 and were to some extent motivated by a paper written by Kenneth R. Shoulders (28). Shoulders outlined a program in which the end point was the production of a computer which would economically perform many of the functions of an intelligent technician. The computer Shoulders envisaged contains 10^{11} components approaching the complexity of the human brain and occupies a volume one inch cubed for easy portability.

The MMP, however, was designed for investigating phenomena and processes which would be useful to the field of thin-film circuitry.

To achieve his goal, Shoulders proposed the use of processors with more than one vacuum station and processes performed in the laboratory atmosphere. Both of these were carefully avoided in the design of the MMP.

The original proposal for the MMP (29) was drawn up in October 1962 and specified that the MMP will permit the controlled deposition of thin films, electron-beam micromachining, topological inspection using a scanning electron microscope and chemical analysis using an electron probe microanalyser. These

processes were to be performed without the need of moving the substrate.

7.1 The Present State of the MMP

The vacuum system which encloses a major part of the MMP has been completed and performed satisfactorily as described in section 6.6.

The main electron beam was operated in the scanning electron microscope mode with a resolution of about one micron. The resolution is at present limited by the performance of the electron gun, which must eventually be replaced both for improved resolution in the scanning microscope and for increased beam power for machining.

For microanalysis, another electron collector similar to the one in use in the scanning microscope will be installed for the type of work as described in section 1.3.2.

A design for the ion beam deposition system has been worked out with special attention paid to the mechanism for bending the ion beam. Bending of the ion beam allows the ion source to be located off the main axis of the MMP.

7.2 Experimental-Research Projects

So far, not much has been said concerning the proposed use of the MMP. Since the MMP was designed to support experimental research, any proposal must of necessity be to

some degree speculative. However, some indication of the type of work planned will be given.

7.2.1 The Preparation of Thin Films

At present, thin films used for integrated circuits are primarily produced by sputtering. To gain reproducible characteristics in the production of these films, variations in the film properties were overridden by fairly heavy "doping". Later, electrical characteristics of the films were controlled by doping, but the use of pure films in thin-film integrated circuits was given up primarily because of the lack of reproducibility.

The first experiments with the deposition system of the MMP will be the preparation of high-purity films and the analysis of their characteristics using the microanalyser and the scanning electron microscope.

Techniques for directly depositing dielectric films have not as yet been developed. Most dielectric films used in thin-film circuits are still produced by chemical or electrolytic anodization.

The quality of dielectric films produced with a partial pressure of oxygen in the deposition system will be investigated.

7.2.2 The Resolution of Micromachining

The importance of the resolution of machining was

discussed in section 4.1. Experiments in machining will be closely associated with the design of a new gun for the MMP.

7.2.3 The Fabrication of Thin-Film Circuits

After the objectives listed in sections 7.2.1 and 7.2.2 have been realized, efforts will be concentrated on the major goal of the MMP project; the fabrication of thin-film circuits using the techniques described.

APPENDIX 1

The FORTRAN Program for the Solution of the Ray Equations

Equation (38) may be rewritten as

$$r'' = \frac{53.5\, r_1^4}{C} \left(\frac{L^2-z^2}{z}\right) \frac{1}{r^3} + \frac{9.6 \times 10^{-4}\, I}{C^{3/2}} \left(\frac{L^2-z^2}{z}\right)^{3/2} \frac{1}{r}$$

$$- \left[\frac{3L^2 + z^2}{2(L^2-z^2)^2} + \frac{53.5}{C}\left(\frac{L^2-z^2}{z}\right)\right] r - \left[\frac{L^2+z^2}{2z(L^2-z^2)}\right] r' \qquad (38a)$$

The voltage V_1 was taken as-20 kv. C is a multiplying coefficient of 20 kv. I is the beam current in microamperes.

A listing of the FORTRAN program used in the solution of equation (38a) follows:

```
C     PROGRAM FOR FULL RAY EQUATION.
      SL=.004225
      TSL=SL+SL
   14 PRINT 18
   18 FORMAT (1H ,4H SET)
      READ 1,DZ,C,I,Z,R,RD,ZFI
    1 FORMAT (7F10.0)
      BC=53.50/C
      PR=C**1.5
      AC=(.00096*I)/PR
      PR=R*R
      PR=PR*PR
      RC=BC*PR
      PRINT 16,I,C,DZ,Z,R
   16 FORMAT (1H ,3H I=,F10.3,3H C=,F10.1,4H DZ=,F8.5,3H Z=,
     F10.5,3H R=,1F8.4)
      PRINT 17
   17 FORMAT (1H ,5X,2H Z,12X,2H R,14X,3H RD,11X,4H RDD)
   15 ZN=Z
      RN=R
      RDN=RD
      N=1
   10 SZ=ZN*ZN
      SUM=SL+SZ
      DI=SL+SZ
      Q=SUM/DI
      Q=Q/ZN
      T=DI/ZN
      V=T**1.5
      Y=.5*((TSL+SUM)/(DI*DI))+BC*T
   12 RB=RN*RN*RN
   11 RDD=(RC*T/RB)+(AC*V/RN)-Y*RN-.5*Q*RDN
      GO TO (4,5,6,7),N
    4 PRINT 9,Z,R,RD,RDD
    9 FORMAT (1H ,F10.6,3E15.7)
      IF (Z-ZFI) 13,14,14
   13 CK1=DZ*RDD
      ZN=Z+.5*DZ
      RN=R+.5*DZ*RD+.125*DZ*CK1
      RDN=RD+.5*CK1
      N=2
      GO TO 10
    5 CK2=DZ*RDD
      RDN=RD+.5*CK2
      N=3
      GO TO 11
    6 CK3=DZ*RDD
      ZN=Z+DZ
      RN=R+DZ*RD+.5*DZ*CK3
      RDN=RD+CK3
      N=4
      GO TO 10
    7 CK4=DZ*RDD
```

```
DR=DZ*(RD+.1666667*(CK1+CK2+Ck3))
DRD=.1666667*(CK1+2.*(CK2+CK3)+CK4)
Z=Z+DZ
R=R+DR
RD=RD+DRD
GO TO 15
END
```

The program for the solution of equation (39) is effectively the same as the previous program with the appropriate statements removed and statement 11 changed to include only the space charge term. A listing follows.

```
C       SPACE CHARGE TERM ONLY
        SL=.004225
     14 PRINT 18
     18 FORMAT (1H ,4H SET)
        READ 1,DZ,C,I,Z,R,RD,ZFI
      1 FORMAT (7F10.0)
        PR=C**1.5
        AC=(.00096*I)/PR
        PRINT 16,I,C,DZ,Z,R
     16 FORMAT (1H ,3H I=,F10.3,3H C=,F10.1,4H DZ=,F8.5,3H Z=,
       F10.5,3H R=,1F8.4)
        PRINT 17
     17 FORMAT (1H ,5X,2H Z,12X,2H R,14X,3H RD,11X,4H RDD)
     15 ZN=Z
        RN=R
        RDN=RD
        N=1
     10 SZ=ZN*ZN
        DI=SL-SZ
        T=DI/ZN
        V=T**1.5
     11 RDD=AC*V/RN
        GO TO (4,5,6,7),N
      4 PRINT 9,Z,R,RD,RDD
      9 FORMAT (1H ,F10.6,3E15.7)
        IF (Z-ZFI) 13,14,14
     13 CK1=DZ*RDD
        ZN=Z+.5*DZ
        RN=R+.5*DZ*RD+.125*DZ*CK1
        RDN=RD+.5*CK1
        N=2
        GO TO 10
      5 CK2=DZ*RDD
        RDN=RD+.5*CK2
        N=3
        GO TO 11
      6 CK3=DZ*RDD
        ZN=Z+DZ
        RN=R+DZ*RD+.5*DZ*CK3
        RDN=RD+CK3
        N=4
        GO TO 10
      7 CK4=DZ*RDD
        DR=DZ*(RD+.1666667*(CK1+CK2+CK3))
        DRD=.1666667*(CK1+2.*(CK2+CK3)+CK4)
        Z=Z+DZ
        R=R+DR
        RD=RD+DRD
        GO TO 15
        END
```

APPENDIX 2

Design of the Magnet Coils

The total mmf. required for the magnetic flux density is 61,200 ampere-turns or 30,600 ampere-turns per coil.

The cross sectional area provided for the turns in each coil is $2\frac{7}{16}" \times 1\frac{13}{16}"$.

Using $\frac{1}{8}"$ outer diameter copper tubing with 0.032" wall thickness and 0.0016" insulation, each coil will accommodate 17 layers of 14 turns and 2 layers of 12 turns because of the notch in the coils. This gives a total of 262 turns. The turns are not staggered so as to provide extra space for cooling.

The current required is, therefore,

$$I = \frac{30600}{262}$$

$$= 116.8 \text{ amps.}$$

The average diameter of the coils is

$$D_{av.} = \frac{13/16 + 5\ 7/16}{2}$$

$$= 3.125"$$

therefore, the total length of tubing required per coil is

$$L = \frac{262 \times 3.142 \times 3.125}{12}$$

$$= 214.4 \text{ feet.}$$

The area of cross-section of the copper tubing is

$$A = \frac{\pi}{4} (0.125^2 - 0.061^2)$$

$$= 9.34 \times 10^{-3} \text{ sq. inch}$$

The resistance of each coil is

$$R = \frac{1.72 \times 10^{-6} \times 214.4 \times 12}{9.34 \times 10^{-3} \times 2.54}$$

$$= 0.186\ \Omega$$

$1.72 \times 10^{-6}\ \Omega$ - cm is the resistivity of copper.

The power dissipated per coil is

$$P = 116.8^2 \times 0.186$$

$$= 2.54 \text{ kw.}$$

Assuming a temperature rise T of 40 C° in the cooling water, the flow required is given by

$$G = \frac{2540 \times 60}{J \times T}$$

$$= 912 \text{ cc/min.}$$

$$= 0.2 \text{ gal./min.}$$

where J = 4.18 joules/calorie.

REFERENCES

1. A.H. Andrews, "An Automated Microcircuit E.B. Processor", Proc. of the Electron Beam Symposium Fifth Annual Meeting, Boston, Mass., pp. 149-157; March 1963.
2. Kenneth R. Shoulders, "On Microelectronic Components, Interconnections, and System Fabrication", Aspects of the Theory of Artificial Intelligence, ed. C.A. Muses, Plenun Press, N.Y.; 1962.
3. L. Holland, "Vacuum Deposition of Thin Films", John Wiley and Sons Ltd., New York; 1961.
4. S.P. Wolsky, "Sputtering Mechanisms", Trans. of the Tenth National Vacuum Symposium of the American Vacuum Society, pp. 309-315, The Macmillan Company, New York; 1963.
5. N. Schwartz, "Reactive Sputtering", Trans. of the Tenth National Vacuum Symposium of the American Vacuum Society, pp. 325-334, The Macmillan Company, New York; 1963.
6. K. Norsworthy, "Ion Beam Deposition - Microelectronic Application", paper presented at the Symposium on Electron Beam Techniques for Microelectronics, Ministry of Aviation, Royal Radar Establishment, Malvern, England; July 6, 7 and 8, 1964.
7. Alfred F. and Erika E. Kaspaul, "Application of Molecular Amplification to Microcircuitry", Trans. of the Tenth National Vacuum Symp., pp. 422-427, The Macmillan Company, New York; 1963.

8. K.H. Steigerwald, "Electron Beam Milling", Proc. 3rd. Symp. on Electron Beam Technology, Boston, Mass., pp. 269-290; March 1961.

9. G. Mollenstedt and R. Speidel, "Newer Developments in Microminiaturization ", Proc. 3rd Symp. on Electron Beam Technology, Boston, Mass., pp.340-357; March 1961.

10. James M. Bridges, "Integrated Electronics in Defence Systems", Proc. of the IEEE, Vol. 52, No. 12, pp. 1405-1411; December 1964.

11. Frank Leary, "Microelectronics", Space/Aeronautics, Vol. 41, No. 2, pp. 68-84; February 1964.

12. S. Kimoto and H. Hashimoto, "The Backscattered Electron Image of the Electron Probe X-ray Microanalyser Using a Silicon P-N Junction as a Detector", Pittsburgh Conference on Analytical Chemistry and Applied Spectroscopy; March 6, 1964.

13. William J. MacDonald, "Vacuum Evaporation by Electron Beam - Some Advantages and Limitations in the Formation of Thin Film Microcircuits", Proc. Fourth Symp. on Electron Beam Technology, Boston, Mass., pp. 372-385; March 1962.

14. Robert Bakish, ed., "Introduction to Electron Beam Technology", John Wiley and Sons Inc., N.Y.; 1962.

15. "Illuminated Wire in Vacuum with Laser", Research and Development, pp. 41-42; December 1964.

16. Marshall I. Nathan and Gerald Burns, "Injection Lasers", Electronics; December 6, 1963.

17. N. Taniguchi and S. Maezawa, "Temperature Analysis of Electron Beam Machining to get the Optimum Operating Condition for Pulsative Method", Proc. of the Electron Beam Symposium Fifth Annual Meeting, pp. 135-148; March 1963.

18. J.R. Pierce, "Theory and Design of Electron Beams", D. Van Nostrand Company, Inc., Princeton, New Jersey; 1954.

19. Cecil E. Hall, "Introduction to Electron Microscopy", Appendix 4.1, p. 78, McGraw-Hill Book Company, Inc., New York; 1953.

20. W.C. Nixon et al., "The "Intercol" Electron Beam System used for Microcircuit Etching", Proc. of the Electron Beam Symposium Fifth Annual Meeting, Boston Mass., pp. 158-167; March 1963.

21. A. Berthelot, "Radiations and Matter", Leonard Hill Limited, London; 1958.

22. L.G. Pittaway, "The Temperature Distribution in Thin Foils and Semi-infinite Targets Bombarded by an Electron Beam", Proc. of the Electron Beam Symposium Fifth Annual Meeting, Boston, Mass., pp.88-123; March 1963.

23. D.B. Langmuir, "Theoretical Limitations of Cathode-Ray Tubes", Proc. of the Institute of Radio Engineers Incorporated, Vol. 25, No. 8, pp.977-991; August 1937.

24. T.E. Everhart, O.C. Wells and C.W. Oatley, "Factors Affecting Contrast and Resolution in the Scanning Electron Microscope", Journal of Electronics and Control, Vol. 7, pp. 97-111; 1960.

25. T.E. Everhart and R.F.M. Thornley, "Wide-Band Detector for Micro-Microampere Low-Energy Electron Current", J.S.I., Vol. 37, pp. 246-248; 1960.

26. P.A. Redhead, J.P. Hobson and E.V. Kornelson, "Ultra-high Vacuum", Advances in Electronics and Electron Physics", Vol. 17, pp. 323-431, Academic Press; 1962.

27. J.G. Needham, "A High Capacity Vacuum Sputtering Machine", Trans. of the Tenth National Vacuum Symposium of the American Vacuum Society, pp. 402-406, The Macmillan Company, New York; 1963.

28. Kenneth R. Shoulders, "Microelectronics Using Electron-Beam - Activated Machining Techniques", Advances in Computers, Vol. 2, pp. 135-293, Academic Press, New York; 1961.

29. G.S. Glinski, W.R. Samaroo and T.J. Mousseau, "Microelectronic Research Laboratory Equipment", Department of Electrical Engineering, The University of Ottawa; October 23, 1962.

VITA

NAME:	Winston Randolph Samaroo
BORN:	San Fernando, Trinidad February 24, 1934
EDUCATED:	
Secondary:	Naparima College, San Fernando, Trinidad.
	Presentation College, San Fernando, Trinidad.
University:	McGill University, Montreal, Canada.
	The University of Ottawa, Ottawa, Canada.
COURSE:	Electrical Engineering
DEGREES:	B.Eng. (McGill) M.Sc. (Ottawa)